CHAPTER IV
RESULTS AND DISCUSSION

In this chapter, we discuss the results of light scattering, conductivity, and viscometric studies of the binary systems of pure polymer and surfactant in aqueous solution (PEO/water and HTAC/water) and the ternary system (PEO/HTAC/water), while investigating the effect of various physical parameters, such as HTAC concentration, PEO concentration, temperature and added salt. Subsequently, the viscoelastic properties of concentrated solutions of pure polymer, pure surfactant, and polymer-surfactant mixtures will be described. Finally, we present an investigation of the interaction between hydroxypropylcellulose polymer (HPC) and the amphoteric surfactant (CADG) interaction.

4.1 Binary System of PEO-Water Mixture

4.1.1 Molecular Weight Measurement

Four PEO specimens with different molecular weights were utilized in viscosity and light scattering measurements, (M_w = 1x10^5 g/mol, 6x10^5 g/mol, 9x10^5 g/mol, and 4x10^6 g/mol), designated as PEO(1), PEO(2), PEO(3), and PEO(4), respectively.

4.1.1.1 Viscosity

Figure 4.1 shows the reduced viscosity (η_{sp}/c_p) for PEO(2) solution as a function of polymer concentration at 30°C. The intercept of the straight line gives the intrinsic viscosity and the slope of the graph yields the Huggins constant according to the Huggins equation (3.5). The Huggins constant (k_H) represents the polymer-polymer interaction in the solvent which is dependent of temperature. The value of k_H lies between 0.2 – 0.5 for flexible polymer coil in good solvent and has a higher k_H value (> 0.5) in poor solvent (Copper, 1989). The reduced viscosity versus polymer concentration graphs for other PEO samples are shown in Appendix (1.1).

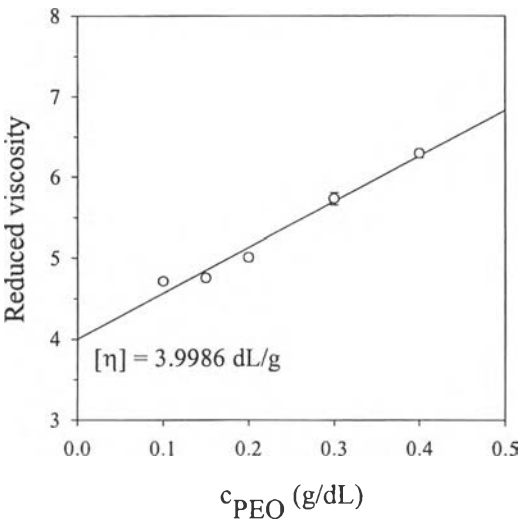

Figure 4.1 Reduced viscosity (η_{red}/c_p) as a function of PEO concentration for PEO(2) solution at 30°C. The intercept of the straight line refers to the intrinsic viscosity.

The intrinsic viscosity and Huggins constant for all PEO samples are tabulated in Table 4.2 together with the values of molecular weight, calculated by using the Mark-Houwink-Sakurada equation (equation 3.7).

4.1.1.2 Light Scattering

Figure 4.2 shows a Zimm plot for the binary system of PEO(2) in water at polymer concentrations ranging from 0.05 to 0.2 g/dL. The Zimm plots for other polymers are shown in the Appendix (1.3). The molecular weight (M_w), radius of gyration (R_g), and the second virial coefficient (A_2) were obtained from dual extrapolations following equation (3.21). Table 4.1 summarizes the Zimm plot results for PEO in water at 30°C. The values of M_w obtained by light scattering are in good agreement with the values quoted by the suppliers and are also consistent with the values obtained from intrinsic viscosity measurements. The R_g values are large which are attributed to the fact that the PEO samples have relatively wide molecular weight distributions.

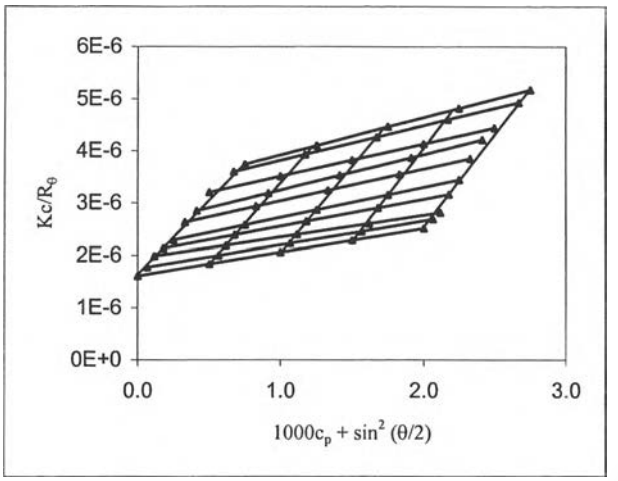

Figure 4.2 Zimm plot for PEO(2) solution in water at 30°C. The lines drawn represent least-squares fit to the data.

Table 4.1 Zimm plot results for PEO in water at 30°C

Polymer*	M_w x 10^{-5} (g/mol)	R_g (nm)	A_2 (mL.mol/g^2)
PEO(1) *1 x 10^5 M_w*	1.23 ± 0.08	41.6 ± 2.8	0.0002 ± 0.0001
PEO(2) *6 x 10^5 M_w*	6.08 ± 0.13	86.8 ± 3.2	0.0002 ± 0.0001
PEO(3) *9 x 10^5 M_w*	9.04 ± 0.32	97.7 ± 2.7	0.0005 ± 0.0001

* *Molecular weight values in italics were provided by the supplier.*

4.1.2 Measurement of Hydrodynamic Radius (R_h)

Figure 4.3 shows the representative plot of the apparent diffusion coefficient (D_{app}) versus the square of scattering wave vector (q^2) at different PEO(2) concentration (0.1 g/dL, 0.2 g/dL, and 0.3 g/dL) by varying scattering angle from 70° to 130°. D_{app} has a linear dependence on q^2 according to equation (3.36). When the apparent diffusion coefficient was extrapolated to zero angle, the center of mass diffusion coefficient was obtained via equation (3.36).

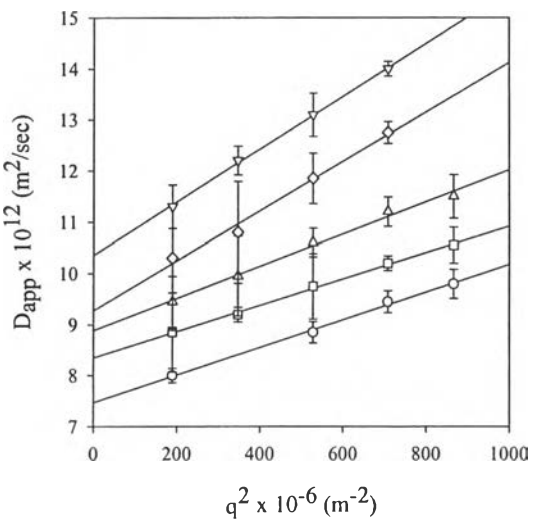

Figure 4.3 Apparent diffusion coefficient (D_{app}) as a function of square of scattering wave vector (q^2) at different PEO concentrations. PEO M_w = 5.97 x 10^5 g/mol, PEO concentration: (O) 0.1 g/dL; (□) 0.2 g/dL; (Δ) 0.3 g/dL; (◊) 0.4 g/dL; and (∇) 0.5 g/dL.

Figure 4.4 indicates the center of mass diffusion coefficient as a function of PEO(2) concentration at 30°C. The PEO concentrations were measured in the dilute concentration range. The diffusion coefficient of infinite dilution (D_0) was obtained from the intercept of the graph, using equation (3.37). The graphs for different molecular weights of PEO are shown in Appendix (1.2). The hydrodynamic radius (R_h) of PEO chain was calculated using the Stokes-Einstein equation (see in equation 3.39).

Table 4.2 displays the values of diffusion coefficient and hydrodynamic radius for all PEO samples obtained from dynamic light scattering, including the results from viscosity measurement.

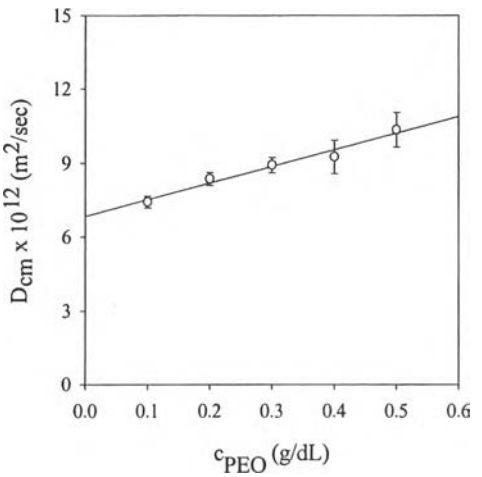

Figure 4.4 Center of mass diffusion coefficient vs. PEO concentration. PEO molecular weight = 5.97 x 10^5 g/mol. The intercept of the straight line refers to the diffusion coefficient at infinite dilution.

Table 4.2 Viscosity and light scattering results for PEO in aqueous solution

Sample	$[\eta]$ (mL/g)	k_H	$^*M_w \times 10^{-5}$ (g/mol)	$D_0 \times 10^{12}$ (m^2/s)	R_h (nm)
PEO(1)	1.0263	0.249	1.04	17.705	15.7
PEO(2)	3.9986	0.354	5.97	6.8370	40.4
PEO(3)	5.4418	0.227	8.86	5.5715	49.8
PEO(4)	17.638	0.258	39.99	-	-

** Molecular weight obtained by viscosity measurement*

4.1.3 dn/dc Measurement

The refractive index increment (dn/dc) of polymer is a necessary prerequisite for the determination of molecular weight. It was determined from the slope of the graph between refractive index versus polymer concentration as shown in Figure 4.5. From the graph, the value of dn/dc was determined to be 0.136 mL/g which is consistent with the value of dn/dc = 0.1357 mL/g, obtained by Polik and Burchard (1983).

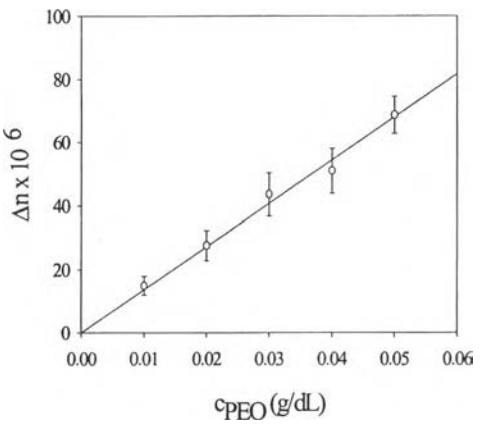

Figure 4.5 Refractive index of PEO as a function of PEO concentration. The slope of the straight line gives the refractive index increment (dn/dc) of the polymer solution.

4.2 Binary System of HTAC Solution

4.2.1 Determination of Critical Micelle Concentration (cmc)

The properties of surfactant solutions are governed by their tendency to minimize the contact of their hydrophobic groups with water. The term of the critical micelle concentration (cmc) refers to the concentration at which surfactant micelles start to occur. In this work, the cmc for HTAC was determined by using both surface tension and conductivity measurements.

4.2.1.1 Surface Tension

Figure 4.6 shows the surface tension versus surfactant concentration plot for HTAC solution which exhibits a significant decrease with HTAC concentration initially, then follows by a sharp break above which the surface tension remains unchanged. From this figure, the cmc of HTAC solution was determined to be 12 mM (0.038 g/dL), which is in good agreement with the value (1.3 mM) reported by Winnik *et al.* (1987). Above the cmc, all of the added HTAC molecules are formed as micelles and therefore the surface tension does not change appreciably.

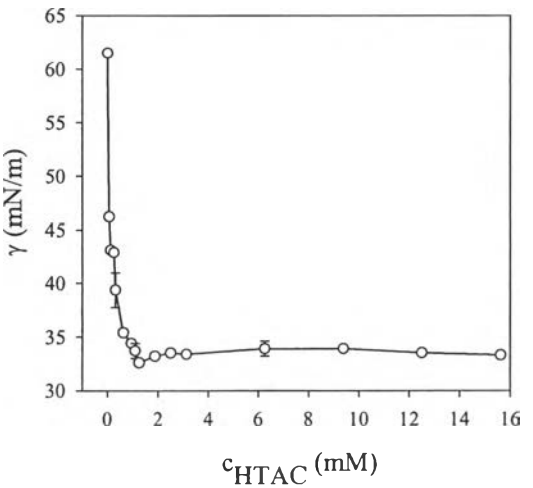

Figure 4.6 Surface tension of HTAC in water as a function of HTAC concentration at 30°C.

4.2.1.2 Conductivity

The determination of cmc by conductivity measurement is shown in Figure 4.7, which is a plot of the conductivity of HTAC, as expressed in μS/cm, as a function of HTAC concentration. The sharp break in the graph represents the cmc which is equal to 1.19 mM. This value is very consistent with that obtained by surface tension measurement and also the value reported by Zana *et al.* (1992). The conductivity versus HTAC concentration graphs for other temperatures are shown in Appendix (2.2). Figure 4.8 shows the variation of conductivity of HTAC solution with HTAC concentration in the presence of 0.1 M KNO_3. The break point represents the cmc of the surfactant solution. It was found that the cmc value for HTAC in salt solution (0.94 mM) is lower than that in water (1.19 mM), which suggests that the surfactant micelles are stabilized in salt solution. The addition of salt leads to a reduction of electrostatic repulsions between the charged surfactant headgroups on micelles, and therefore, the cmc of HTAC in the presence of salt is lower than that in the absence of salt.

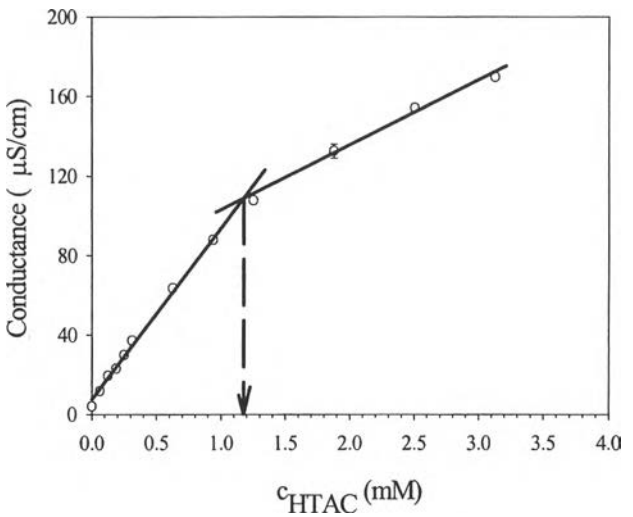

Figure 4.7 Variation of conductivity with HTAC concentration to determine the critical micelle concentration (cmc).

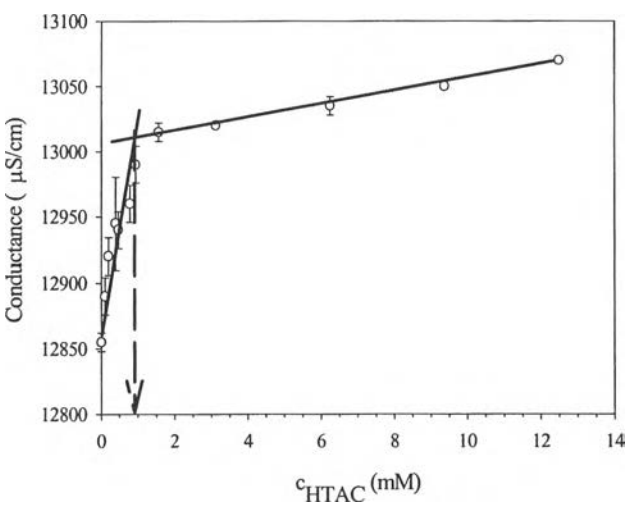

Figure 4.8 Variation of the conductivity of HTAC solution with the HTAC concentration at 30°C in the presence of 0.1 M KNO_3. The break point represents the critical micelle concentration.

4.2.2 Viscosity Measurement

Figure 4.9 shows a semi-logarithmic plot of the specific viscosity of HTAC as a function of HTAC concentration. The increase in viscosity is related to the structure of surfactant micelle. The viscosity of surfactant is approximately equal to that of water at low HTAC concentration. Above the critical micelle concentration (cmc), spherical micelles are formed at low surfactant concentration. At this concentration range, the specific viscosity of HTAC slightly increases with increasing HTAC concentration up to 31.25 mM (1 g/dL) (see in Figure 4.9). Beyond this concentration range, the viscosity increases dramatically, accompanied by a change in the micellar structure from spherical to rod-like (or) cylindrical shape (Porter, 1994). Therefore, the specific viscosity increases four times when the HTAC concentration reaches beyond 100 mM. Imae and Ikeda (1987) showed that spherical surfactant micelles gradually increase in size with an increase in molar concentration of counterion, as measured by dynamic light scattering spectrophotometer.

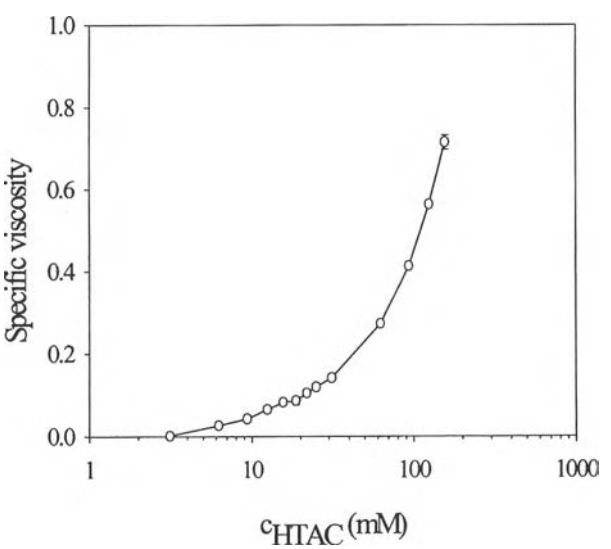

Figure 4.9 Semi-logarithmic plot of the specific viscosity as a function of HTAC concentration.

4.3 Ternary System of PEO/HTAC/Water

In this work, the interaction between PEO and HTAC was characterized by using conductivity, viscosity, and light scattering measurements. The experiments were performed in the PEO concentration range of 0.01 to 0.1 g/dL to determine the effect of PEO concentration and the temperature range of 10 to 50 °C for the effect of temperature measurement. Here, polymer concentration (c_{PEO}) is designated as c_p, surfactant concentra- tion (c_{HTAC}) as c_s, and the concentration ratio of surfactant to polymer (c_{HTAC}/c_{PEO}) as c_s/c_p.

4.3.1 Effect of Surfactant Concentration

To study the effect of surfactant concentration, the polymer concentration was fixed at 0.1 g/dL and the temperature at 30 °C.

4.3.1.1 Conductivity Measurement

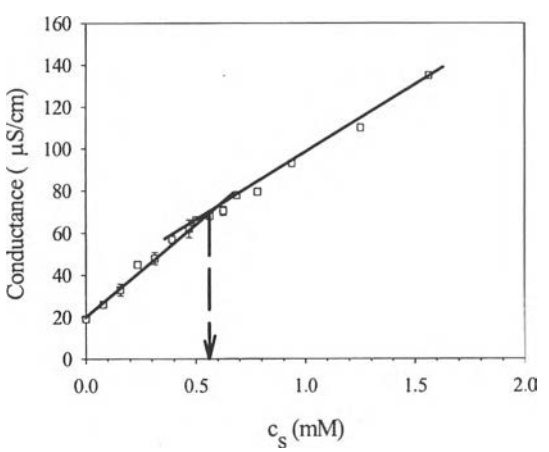

Figure 4.10 Variation of conductivity with HTAC concentration in the presence of PEO(2).

Figure 4.10 shows the variation of the conductivity of HTAC with HTAC concentration in the presence of polymer. The break point represents the critical aggregation concentration (cac) which is the concentration at which polymer-

surfactant aggregates start to form. As seen clearly, the cac (0.56 mM) is smaller than the cmc value (1.19 mM) which indicates the occurrence of interaction between the polymer and the surfactant.

4.3.1.2 Viscosity and R_h Measurements

Figures 4.11 and 4.12 show the specific viscosity and the diffusion coefficient of PEO as a function of HTAC concentration. The hydrodynamic radius (R_h) of PEO was calculated from the diffusion coefficient by using the Stokes-Einstein equation (equation 3. 40). Thus, R_h is inversely proportional to the diffusion coefficient. The corresponding graphs for the determination of R_h values are shown in the Appendix (3). The results of viscosity measurements, shown in the viscosity data, can be divided into three regions.

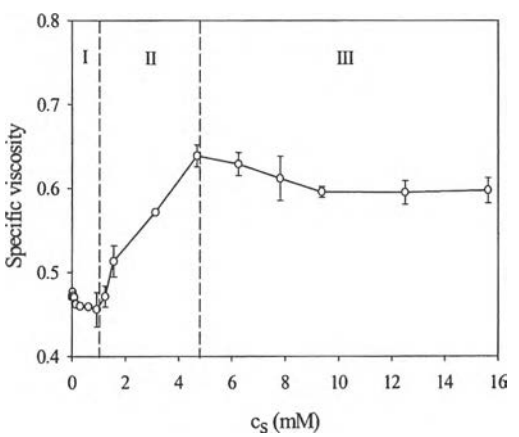

Figure 4.11 Specific viscosity (η_{sp}) as a function of HTAC concentration for PEO(2) solutions.

Region (I): At very low HTAC concentration below cmc, there is adsorption of a few HTAC molecules to the PEO chain, and therefore, chain contraction occurs. A similar phenomenon was observed in the EHEC-SDS system, reported by Hoff *et al.* (2001), who reported that a strong contraction of the EHEC-SDS complex occurred at the onset of surfactant binding to the polymer. At this stage, micelles begin to form inside the polymer, accompanied by the collapse of the polymer chain because of the cooperative binding of surfactant molecules.

Region (II): When the HTAC concentration exceeds the cac value, η_{sp} and R_h substantially increase up to the maximum binding point, because of the electrostatic repulsions between the HTAC micelles bound to the PEO, which leads to chain expansion. At the maximum binding point, the polymer chains are saturated with HTAC micelles. Similar observations have been made in several polymer-surfactant complex systems (Nilsson, 1995; Chari *et al.*, 1994).

Region (III): Beyond the saturation point, a decrease in η_{sp} and R_h are observed because of a decrease in the electrostatic repulsion between the charge particles due to the large amount of counterions (Cl^-) in the solution, i.e. the electrostatic screening effect. This would induce a strong reduction in the hydrodynamic size of the PEO chain and at the same time reduce the viscosity. A similar situation was evident in the work of Fundin *et al.* (1997), who reported light scattering results for PAA-CTAB system. They attributed that a single PAA chain binds several CTAB micelles to form a complex. At very high CTAB concentration, free micelles coexist with the complexes. Therefore, the hydrodynamic radius of the complex is reduced by the screening effect of free micelles.

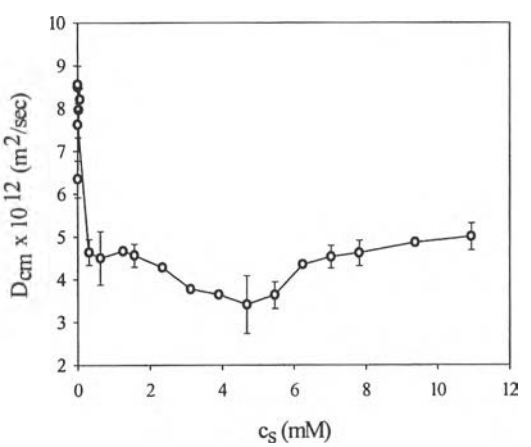

Figure 4.12 Center of diffusion coefficient (D_{cm}) as a function of HTAC concentration for PEO(2) solution. PEO concentration: 0.1 g/dL.

4.3.2 Effect of Polymer Concentration

To study the effect of PEO concentration, the viscosity and R_h measurements were performed in the PEO concentration range of 0.01 to 0.1 g/dL and the surfactant concentration was varied from 0 to 16 mM. The temperature was fixed at 30°C.

4.3.2.1 Viscosity Measurement

Figures 4.13 and 4.14 show the specific viscosity (η_{sp}) of polymer in PEO-HTAC system as functions of the HTAC concentration and the mass concentration ratio of HTAC/PEO for different PEO concentrations. These figures indicate that η_{sp} increases with increasing PEO concentration. At fixed PEO concentration, an increase in η_{sp} was observed by increasing HTAC concentration until the saturation point and then η_{sp} decreases again. This phenomenon was explained in the previous section (Section 4.3.1.2).

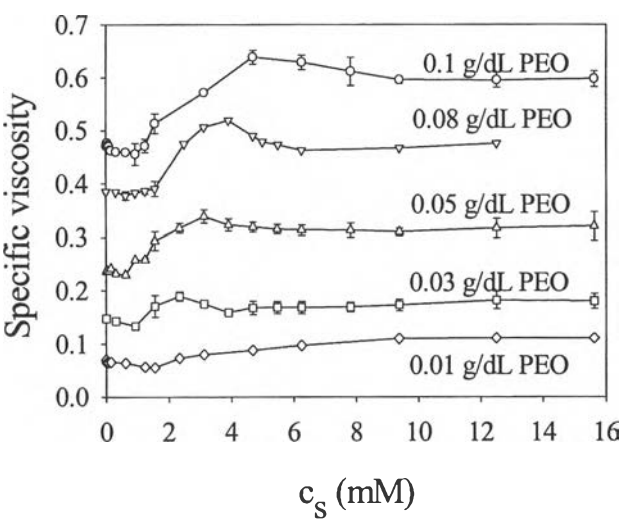

Figure 4.13 Dependence of specific viscosity on surfactant concentration at different polymer concentrations: (∇) 0.01 g/dL; (◊) 0.03 g/dL; (Δ) 0.05 g/dL; (□) 0.08 g/dL; and (O) 0.1 g/dL.

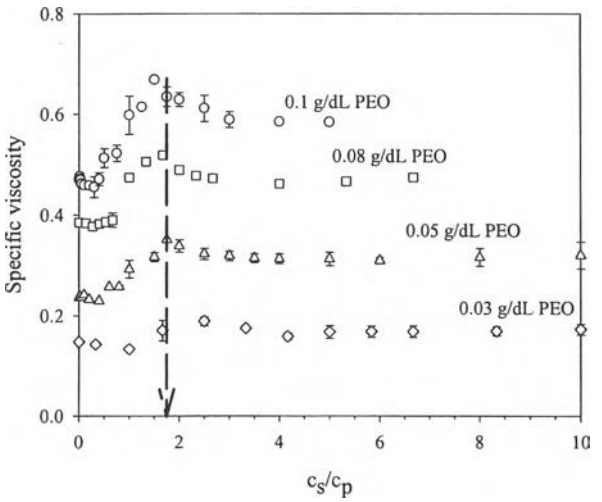

Figure 4.14 Dependence of specific viscosity on c_s/c_p ratio at different PEO concentrations.

As seen in Figure 4.13, the maximum binding points shift to a higher surfactant concentration as increasing PEO concentration, suggesting that the greater the number of PEO chains in the solution, the more surfactant is required to bind polymer to obtain maximum binding. The binding saturation concentrations of HTAC together with the concentration ratios of HTAC/PEO at various PEO concentrations are tabulated in Table 4.3.

As shown in Table 4.3, the maximum binding points exist the concentration ratio between 1.5 to 2.0. At the lowest PEO concentration (0.01 g/dL), no apparent saturation concentration is observed. The viscosity maximum is also very weak in 0.03 g/dL PEO concentration and thus the saturation point for this concentration was neglected. Therefore, the average maximum binding point is at $c_s/c_p = 1.75$ (see Fig. 4.1.4). This value was used to determine the structure of PEO-HTAC complex at the maximum binding point, which will be discussed later.

Table 4.3 The saturation concentrations of HTAC and the saturation ratios of HTAC/PEO at different PEO concentrations

PEO (g/dL)	$[HTAC]_{sat}$ (mM)	$[HTAC/PEO]_{sat}$
0.01	-	-
0.03	2.4	-
0.05	3.2	2.0
0.08	4.0	1.75
0.10	5.0	1.5

$[HTAC]_{sat}$ = The saturation concentration of HTAC

$[HTAC/PEO]_{sat} = [c_s/c_p]_{sat}$ = The saturated mass concentration ratio of HTAC to PEO

4.3.2.2 R_h Measurement

Figure 4.15 shows the mean diffusion coefficient as a function of HTAC concentration at different PEO concentrations. The diffusion coefficient of PEO decreases upon addition of HTAC until it reaches a minimum, corresponding to the formation of a saturated PEO-HTAC complex. Thus, the R_h values of the PEO in the PEO-HTAC complex, determined using the Stokes-Einstein equation exhibit a maximum, as shown in Figure 4.16. In this Figure, the R_h increases as increasing PEO concentration. The maximum binding point, found in R_h measurement, is well consistent with the value obtained in the viscosity measurement. A similar observation has been reported in the work of Treiner and Nguyen (1990), who investigated the interaction of PEO and PVP with the anionic surfactant, copper dodecylsulphate $[Cu(DS)_2]$.

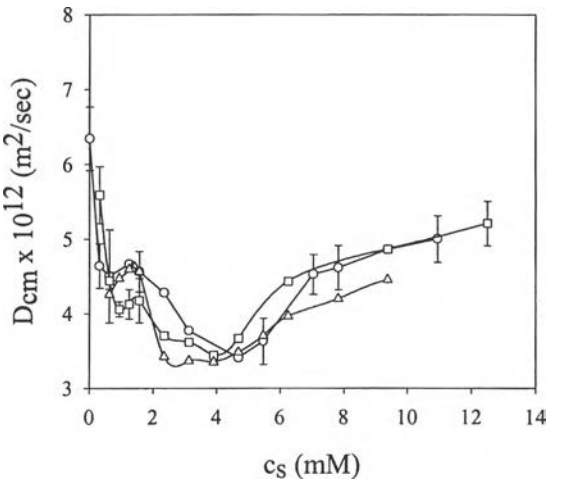

Figure 4.15 Diffusion coefficient as a function of surfactant to polymer concentration ratio (c_s/c_p). PEO concentrations: (Δ) 0.05 g/dL; (□) 0.08 g/dL; (O) 0.1 g/dL.

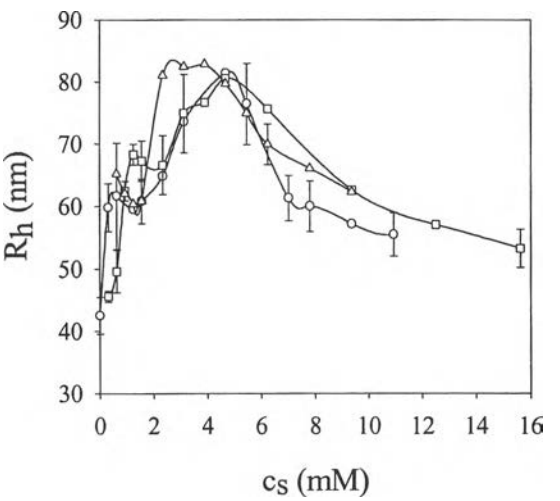

Figure 4.16 Hydrodynamic radius (R_h) as a function of surfactant to polymer concentration ratio (c_s/c_p). The symbols shown here are the same as Figure 4.15.

4.3.3 Effect of Temperature

4.3.3.1 Measurements of cmc and cac

Figure 4.17 shows the variation of the cmc and the cac as a function of temperature in the solutions of HTAC in water and in a PEO-water mixture using conductivity measurements. The plots for the conductivity versus HTAC concentration for each temperature are shown in the Appendix. The polymer concentration was fixed at 0.1 g/dL [M_w = 5.97 x 10^5 g/mol], and the HTAC concentration was varied in all experiments. Within the temperature range of 25°C-50°C, the cmc does not vary, whereas the cac decreases rapidly as temperature increases above 25°C, indicating an increasingly strong interaction between PEO and HTAC. At 25°C, the cmc and the cac values are essentially identical, indicating that negligible interaction takes place between PEO and HTAC at or below 25°C.

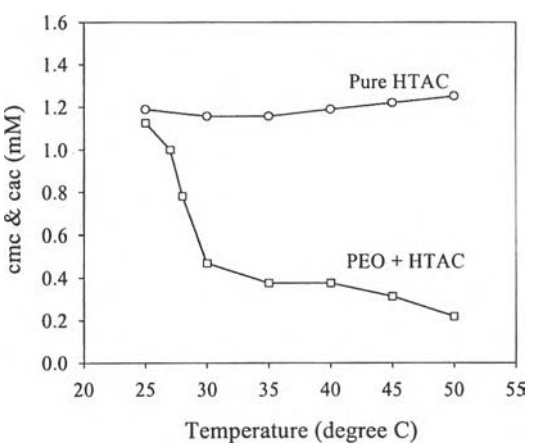

Figure 4.17 Variation of the cmc and the cac with temperature for HTAC in water and in the presence of PEO.

This result contrasts with the observations of Anthony and Zana (1994) that the onset of an interaction between PEO and TTAB occurs only at temperatures above 35°C. The decrease in cac with rising temperature can be expressed in terms of a reduction in the free energy of micellization. Using the phase

separation model (Tanford, 1980) as a first approximation and neglecting changes in micelle size, the reduction in free energy can be defined as,

$$\Delta G = - RT \ln [cmc/cac]. \qquad (4.1)$$

From the above equation, it was calculated how much PEO lowers the free energy of micellization in units of RT and found that the reduction in free energy is 0.05 RT units at 25°C, which increases to 1.74 RT units at 50°C.

4.3.3.2 Viscosity Measurement

Figure 4.18 shows the variation of the specific viscosity with surfactant concentration at four different temperatures. At low surfactant concentration, the specific viscosity decreases slightly with increasing temperature (see the insert to Figure 4.18). Here, the concentration of the surfactant is comparable to the cac, and only a few surfactant micelles bound to the polymer. PEO becomes less polar with increasing temperature, and hence, the chain contracts, resulting in a decrease in specific viscosity.

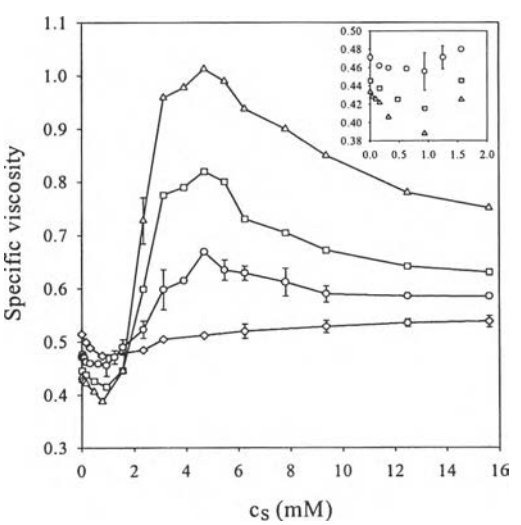

Figure 4.18 Dependence of specific viscosity on HTAC concentration at four different temperatures: (◊) 25°C; (O) 30°C; (□) 40°C; and (Δ) 50°C.

At higher surfactant concentrations, an increase in solution specific viscosity is observed with increasing temperature. This indicates that a sufficient number of surfactant micelles bound to PEO to produce a chain expansion due to electrostatic repulsions between bound micelles. In this figure, the increase in viscosity is more pronounced at higher temperatures, i.e., the chain expansion is larger at higher temperatures. This result indicates that a substantial increase in the amount of charge carried by bound micelles occurs on increasing temperature, which increases the strength of electrostatic repulsions. At a certain surfactant concentration, the specific viscosity reaches a maximum but then decreases with a further increase in HTAC concentration. The viscosity maximum has been interpreted (Chari *et al.*, 1994) to indicate the point at which PEO chains are saturated with surfactant micelles. The decrease in viscosity above the saturation point was interpreted (Chari *et al.*, 1994) as due to the effect of added counterions (Cl^-) in screening the repulsive interactions among micelles bound to the PEO chains. These results are generally consistent with the findings of previous studies (Lindman *et al.*, 1990; Zana *et al.*, 1992; and Anthony and Zana, 1994), which indicate that a less polar polymer segment provides a better nucleus for surfactant self-assembly and that increase in temperature leads to a decrease in polarity and, hence, a more effective interaction between polymer and surfactant.

An interesting feature of Figure 4.18 is that the position of the maximum in specific viscosity is independent of temperature, occurring at around 5 mM HTAC. This indicates that the saturation concentration of binding is independent of temperature. This result agrees with previous findings that the saturation concentration of binding of an ionic surfactant to a polymer is only weakly dependent on polymer hydrophobicity (Anthony and Zana, 1994).

Figure 4.19 shows the comparison between the temperature dependence of specific viscosity (η_{sp}) at HTAC concentrations below the cac and the temperature dependence at concentrations far above the cac. Clearly, η_{sp} decreases below the cac with temperature, whereas above the cac, η_{sp} increases sharply with temperature. The variation in viscosity in dilute solution is dictated primarily by the hydrodynamic volume of the polymer chain, assuming no intermolecular association

of chains. In the binary system of PEO in water, η_{sp} decreases as increasing temperature. This behavior is well understood for PEO in aqueous solution (Kroschwitz, 1996). The PEO chains are assumed to be a more compact conformation at elevated temperatures, presumably because the poorer solvation of the PEO outweighs any weak electrostatic repulsions at higher temperature.

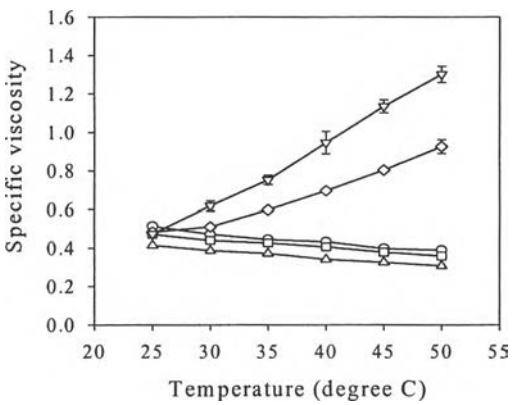

Figure 4.19 Temperature dependence of specific viscosity on surfactant concentration. (0) pure PEO(2) solution; (□) 0.16 mM; (Δ) 0.5 Mm; (◊) 2.5 mM; and (∇) 5 mM.

Also evident in Figure 4.19 is that as a small amount of surfactant ($c \leq$ cmc) is added to the polymer solution at a fixed temperature, η_{sp} decreases relative to the viscosity of the pure polymer solution. Such a decrease has been observed in our previous work (Mya *et al.*, 1999) at a surfactant concentration lower than one micelle per polymer coil. Above the cac and at a fixed temperature, η_{sp} increases with surfactant concentration, obviously due to electrostatic repulsions between the bound micelles. At 25°C, a particular behavior was observed, no variation in η_{sp} occurs with surfactant concentration when it is well above cmc, suggesting a small or negligible interaction between the PEO and the HTAC. This result is consistent with that observed in the conductivity measurement (Figure 4.17). At the saturation point of binding (c_{HTAC} = 5 mM, Figure 4.18), η_{sp} increases most steeply with temperature, indicating that the electrostatic repulsion becomes most

pronounced at the maximum binding condition. The present results can be compared with those of Anthony and Zana (1994), who observed an interaction between PEO and TTAB only at temperatures above 35°C. Thus, it appears that the more hydrophobic HTAC has a greater tendency for association with PEO.

4.3.3.3 Hydrodynamic Radius (R_h) Measurement

Figure 4.20 shows the apparent hydrodynamic radius (R_h) determined from the dynamic light scattering experiments as a function of surfactant concentration at each temperature. R_h was calculated from equation (3. 40) using D_{cm}. Evidently, as surfactant is added, R_h increases to a maximum value, which occurs at a surfactant concentration similar to that of the specific viscosity, and then decreases again. The magnitude of the increase in R_h is larger at higher temperature, again consistent with the viscosity data. These data confirms that the polymer coil expands as temperature and the surfactant concentration increases beyond the cac due to the binding of surfactant micelles to the PEO coils. Thus, the dynamic light scattering results substantiates the interpretation of the viscosity measurements. The location of the maximum in the hydrodynamic radius corresponds to the maximum binding between PEO and HTAC. Beyond the saturation point, the hydrodynamic radius of polymer chain decreases due to the screening effect of Cl^- counterions from the excess surfactant solution.

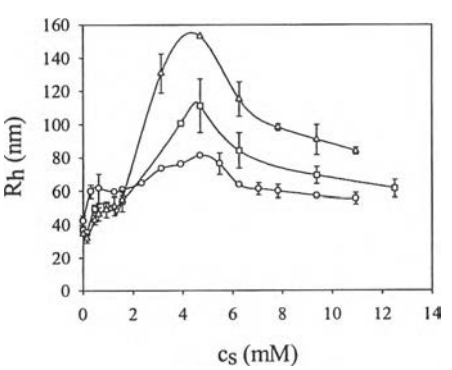

Figure 4.20 Apparent hydrodynamic radius (R_h) as a function of HTAC concentration at three different temperatures. (O) 30°C; (□) 40°C; (Δ) 50°C.

4.3.4 Effect of Molecular Weight

To explore the effect of polymer molecular weight, the concentration of PEO was fixed at 0.1 g/dL at 30°C, and the HTAC concentration was varied.

4.3.4.1 Viscosity Measurement

Figure 4.21 shows the dependence of specific viscosity on the surfactant concentration at four different polymer molecular weights. In each case above the cac, η_{sp} increases due to the expansion of the PEO coil upon binding with surfactant micelles. The viscosity maximum is more prominent with increasing polymer molecular weight. This is expected because the hydrodynamic volume is an increasing function of molecular weight, e.g., for flexible coils, $\eta_{sp} \sim M^a$, with $0,5 < a < 0.8$, depending on solvent quality (Bailey and Koleske, 1976).

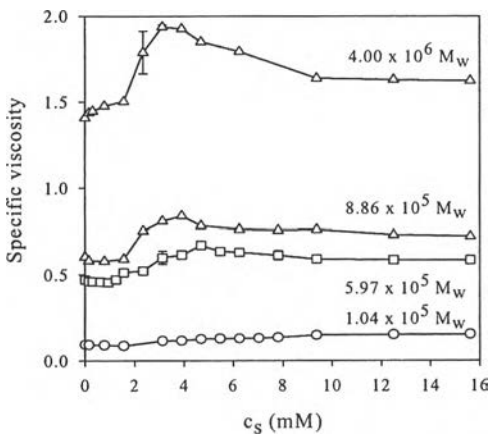

Figure 4.21 Dependence of specific viscosity on HTAC concentration at four different PEO molecular weights: (◊) M_w = 1.04 x 10^5 g/mol; (O) M_w = 5.97 x 10^5 g/mol; (□) M_w = 8.86 x 10^5 g/mol; (Δ) M_w = 4.00 x 10^6 g/mol.

Figure 4.22 indicates the ratio η_{sp} (PEO + HTAC)/ η_{sp} (PEO) as a function of the surfactant concentration. There is approximate superposition of the data, with the exception of the lowest molecular weight (1.04 x 10^5 g/mol), for which the viscosity change is perhaps too small to measure accurately. Also in Figure 4.21, the position of the viscosity maximum is only weakly dependent on the PEO

molecular weight, decreasing slightly as molecular weight increases. Thus, the mole ratio of the HTAC/PEO repeating unit at the saturation point decreased slightly with molecular weight, having a value of approximately 0.2 mole of HTAC/mole of PEO repeating unit for M_w = 5.97 x 10^5 g/mol (weight ratio: 1.5 g of HTAC/g of PEO), 0.17 mole of HTAC/mole of PEO repeating unit for M_w = 8.86 x 10^5 g/mol (weight ratio: 1.2 g of HTAC/g of PEO), and 0.15 mole of HTAC/mole of PEO repeating unit for M_w = 4.00 x 10^6 g/mol (weight ratio: 1.125 g of HTAC/g of PEO).

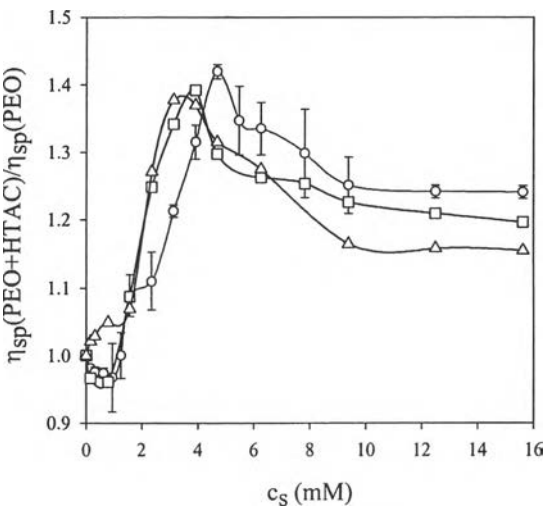

Figure 4.22 The ratio of η_{sp}(PEO+HTAC)/η_{sp}(PEO) as a function of HTAC concentration.

Assuming the aggregation number of HTAC micelles to be 75, as reported by Zana *et al.* (1992), this result implies there are 37 micelles per PEO chain when M_w = 5.97 x 10^5 g/mol, 44 micelles per PEO chain when M_w = 8.86 x 10^5 g/mol, and 185 micelles per PEO chain when M_w = 4.00 x 10^6 g/mol. Note that this calculation gives an upper limit to the number of bound micelles, since it assumes all HTAC micelles are bound to PEO and there are no free micelles in the solution. The decrease in the saturation weight ratio of bound HTAC with increase of PEO molecular weight (Figure 4.22) reflects possibly that the probability of a micelle

having multiple attachment sites to the same or different PEO chains increases with increase of molecular weight.

4.3.4.2 Measurement of R_h

Figure 4.23 shows the apparent values of R_h, derived from translational diffusion coefficients measured by dynamic light scattering for various molecular weights of PEO at finite concentrations. The results are again consistent with the viscosity data, exhibiting a maximum at an HTAC concentration which correlates with that observed in the viscosity data. Also, the magnitude of the increase in R_h is, as expected, greater for the higher molecular weights, since for flexible chains, $R_h \sim M^b$, with $0.5 < b < 0.6$ (Devanand and Selser, 1991).

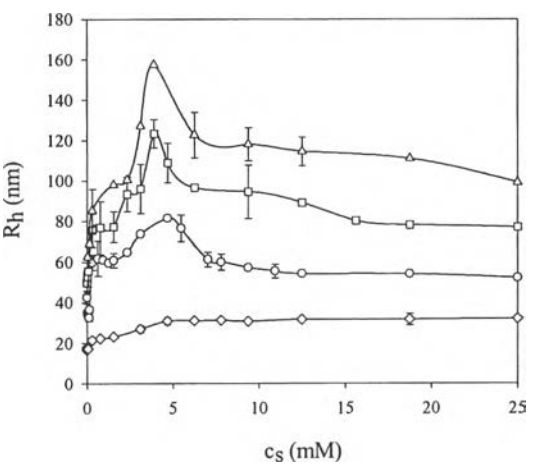

Figure 4.23 Dependence of apparent hydrodynamic radius on HTAC concentration at different PEO molecular weights. The symbols for each molecular weight are shown in Figure 4.21.

4.3.5 Effect of Salt

4.3.5.1 Conductivity Measurement

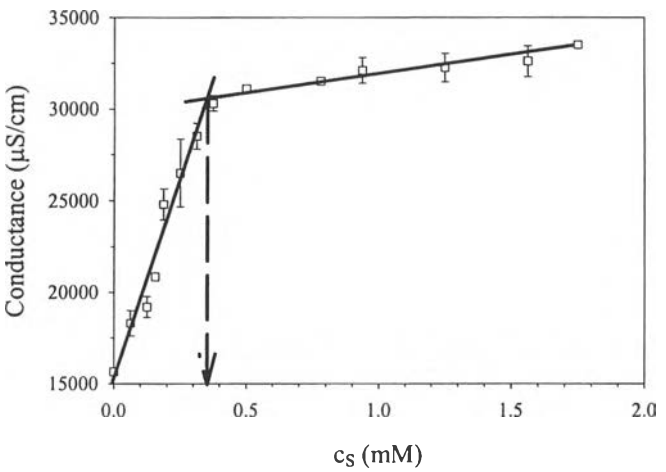

Figure 4.24 Variation of the conductivity of PEO-HTAC complex with HTAC concentration at 30°C in the presence of 0.1 M KNO_3.

Figure 4.24 shows the variation of the conductivity of PEO-HTAC complex with HTAC concentration in the presence of 0.1 M KNO_3 solution. As shown in section 4.2.1.2, the cmc value for HTAC in salt solution (0.94 mM) is lower than that in water (1.19 mM), indicating that the surfactant micelles are stabilized in salt solution. The addition of salt leads to a reduction of electrostatic repulsions between the charged surfactant headgroups on micelles, and also between bound micelles on the polymer. Quantitatively, the strength of interaction can be expressed by means of the Gibbs free energy of micellization in the presence and absence of salt. The reduction in free energy of micelles binding to a polymer was calculated by using equation 4.1. It was determined that the reduction in free energy of polymer-bound micelle is 1.88 kJ/mol of surfactant in water, and increases to 2.53 kJ/mol of surfactant in 0.1 M KNO_3, which confirms that salt-induced electrostatic screening increases the strength of interaction.

4.3.5.2 Viscosity Measurement

Figure 4.25 shows the variation in the specific viscosity of ternary PEO-HTAC solutions in 0.1 M KNO_3, when titrated with HTAC, and compares the results with PEO-HTAC in the absence of added salt. In this measurement, the PEO concentration was fixed at 0.1 g/dL and the HTAC concentration was varied.

The viscosity of the PEO in 0.1 M KNO_3 is slightly lower than that of the PEO in water. This results implies that the polymer conformation had changed by the addition of salt. The salt effect was attributed to contraction of the PEO chain because added salt competes with the polymer for the water of hydration due to the breaking of intermolecular hydrogen bonding between polymer and water as reported by Lance-Gomez and Ward (1986).

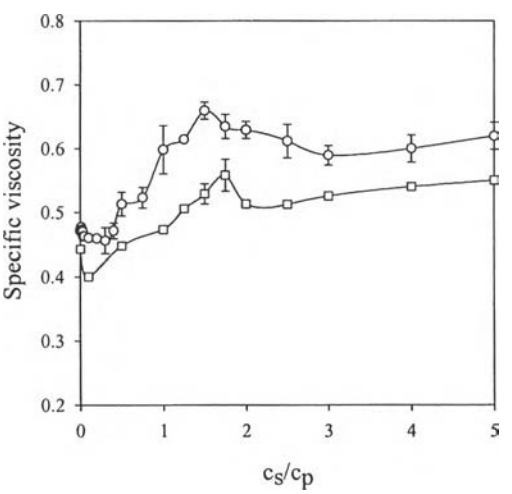

Figure 4.25 Dependence of specific viscosity on HTAC to PEO concentration ratio in water (O); and in the presence of 0.1 M KNO_3 solution (□). PEO concentration: 0.1 g/dL.

As evident in Figure 4.25, when PEO is titrated with HTAC in 0.1 M KNO_3, after the initial dip, η_{sp} increases up to a maximum value, and then decreases slightly, essentially mirroring the behavior earlier seen in the absence of

salt, also shown in Figure 4.25. Two differences evident are that the magnitude of the viscosity variation is smaller, and the location of the peak maximum is at a slightly higher concentration ratio, in 0.1 M KNO_3. The first observation is qualitatively consistent with the interpretation of the viscosity maximum as an increase in hydrodynamic radius (R_h), (Hormnirun *et al.*, 2000) because of electrostatic repulsions between the bound micelles. The chain expansion is substantially reduced in 0.1 M KNO_3, because of screening of the electrostatic repulsions. This result is also in agreement with previous studies (Brown *et al.*, 1992; Anthony and Zana, 1994), which found that the strongest coil expansion was observed at lowest concentration of added salt. The second observation is in agreement with reports by Cabane and Duplessix (1982) and Francois *et al.*, (1985) that the binding ratio of SDS to PEO increases with increasing ionic strength.

In contrast, the conductivity data shown in section 4.3.5.1 indicates that the strength of interaction is greater in salt solution than in aqueous medium. It is noted that the viscosity reflects the conformational change of the polymer rather than the strength of the complex formation (Gilyani and Wolfram, 1985). A similar observation was found in PEO-SDS system reported by Francois *et al.* (1985), who observed the reduction in reduced viscosity by adding salt. The charge density of the polyelectrolyte complex is reduced by adding salt, but the binding ratio of surfactant to polymer (~ 0.3 mol SDS per mol EO) increases with added salt. Greener *et al.* (1987) observed a maximum in viscosity of alkali-processed gelatin on titration with SDS, interpreted as due to cross-linking of gelatin chains by SDS micelles.

4.3.6 Determination of the Structure of PEO-HTAC Complex

4.3.6.1 PEO-HTAC Complex in Water

To avoid any change in the structure of the complex upon varying polymer and surfactant concentration, static light scattering measurements were performed at constant ratio of HTAC to PEO(2) (i.e. constant c_s/c_p). The maximum binding ratio of HTAC to PEO(2), which has $M_w = 6.08 \times 10^5$ g/mol, as determined by static light scattering, occurred at $c_s/c_p \sim 1.75$. The molecular weights of PEO in the PEO-HTAC complex at different c_s/c_p ratios by light scattering

analysis via equation (3.27), using the $(dn/dc_p)_{\mu s}$ values after equilibrium dialysis, are listed in Table 4.4. The corresponding Zimm plot for the PEO(2)-HTAC complex at c_s/c_p = 1.75, constructed following equation (3.27), is shown in Figure 4.26. As evident in Table 4.4, M_w increases up to the maximum binding point at c_s/c_p = 1.75, indicative of an increasing level of interpolymer complex formation. Above c_s/c_p = 1.75, M_w levels off, indicating that excess surfactants do not reduce the tendency that PEO chains to share micelles.

Then, the preferential binding (D') of HTAC to PEO(2) at different concentration ratios was determined, using equation (3.11), combining values of $(dn/dc_p)_{\mu s}$ with $(dn/dc_p)_{cs}$ and $(dn/dc_s)_{cp}$ values, respectively, from equations (3.9) and (3.10). Subsequently, $M_{w,com}$ was computed through equation (3.28). The corresponding values of $(dn/dc_p)_{\mu s}$, $(dn/dc_p)_{cs}$, $(dn/dc_s)_{cp}$, M_w, D' (in grams HTAC/ gram PEO, and in moles HTAC/mole EO), and $M_{w,com}$ were each displayed in Table 4.4. Above the cac ($c_s/c_p \sim 0.1$), $M_{w,com}$ increases steeply with added HTAC up to the maximum binding point, where it levels off. This increase derived from two sources, an increase in D', and the previously-mentioned increase in M_w. From the latter, on average, 2.0 ± 0.3 PEO chains are involved in formation of the PEO-HTAC complex at maximum binding.

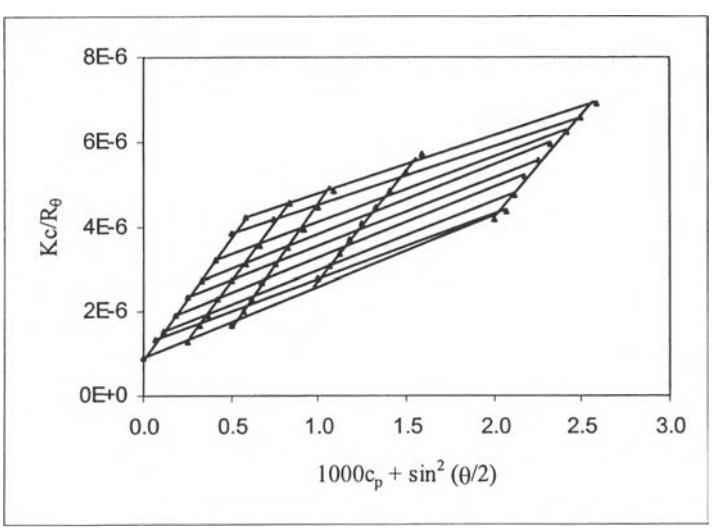

Figure 4.26 Zimm plot for PEO(2)-HTAC complex solution at the maximum binding point (c_s/c_p = 1.75). The lines are drawn by least-squares fit method.

In addition, $N_{s,b}/N_p$, the number of bound HTAC molecules per PEO(2) chain, was determined from equation (3.28) as $N_{s,b}/N_p = D'M_{w,PEO}/M_{HTAC}$, where $M_{w,PEO}$ = 608,000, and M_{HTAC} = 319 g/mole is the molecular weight of HTAC. The results are shown in Table 4.5 and compared with N_s/N_p, the total number of HTAC molecules (bound + free HTAC molecules) per PEO(2) chain. The number of free HTAC molecules per PEO chain $N_{s,f}/N_p$, and the number of bound HTAC micelles $n_{s,b}$, are also listed in Table 4.5. The latter computed from the aggregation number of free HTAC micelles, reported by Zana *et al.* (1992). Note that this estimate may be inaccurate, since the aggregation number of bound micelles is lower than that of free micelles, although it is reported to approach the latter as the surfactant to polymer ratio increases (Whitte and Engberts, 1989). At maximum binding (c_s/c_p = 1.75), only 50% of the available surfactant molecules are bound to the polymer chain (see Table 4.5), thus the complex coexists with free surfactant micelles. This relatively weak binding affinity of HTAC for PEO may be the driving force for PEO chains to share micelles when forming complexes.

Above maximum binding, the amount of bound surfactant appears to decrease significantly. The reason for this is not clear. However, Zimm plot analysis of the light scattering intensities also indicates that the radius of gyration, R_g, of the complex increases with added surfactant up to c_s/c_p = 1.75, and then decreases significantly, as shown in Table 4.6. Thus the decrease in D' and $N_{s,b}/N_p$ above c_s/c_p = 1.75 may reflect some changes in structure of bound micelles which accompanies the decrease in R_g. Also presented in Table 4.6 are values of the hydrodynamic radius, $R_{h,f}$, and polydispersity, μ_2/Γ^2, obtained in dynamic light scattering, as well as approximate values of the viscometric hydrodynamic radius, $R_{h,\eta}$, obtained by combining the viscosity data and the molecular weight information as,

$$\frac{\eta_{sp} M_{w,com}}{c_p(1+D')} \sim 2.5 N_A V_h. \qquad (4.2)$$

Table 4.4 Refractive index increments and molecular weight obtained by thermodynamic treatment method

c_s/c_p	$(dn/dc_p)_{\mu s}$ (mL/g)	$(dn/dc_p)_{cs}$ (mL/g)	$(dn/dc_s)_{cp}$ (mL/g)	D' (g HTAC/g PEO)	D' (mol HTAC/mol EO)	$M_w \times 10^{-5}$ (g/mol)	$M_{w,com} \times 10^{-5}$ (g/mol)
0	0.1362	0	0	0	0	6.08 ± 0.13	6.08 ± 0.13
0.1	0.1440	0.1346	0.1362	0.069	0.009	6.25 ± 0.13	6.54 ± 0.20
0.5	0.1480	0.1202	0.1302	0.214	0.030	6.64 ± 0.18	8.06 ± 0.31
1.0	0.1540	0.1120	0.1173	0.358	0.049	6.80 ± 0.26	9.24 ±0.50
1.75	0.1880	0.1002	0.1005	0.874	0.121	12.07 ± 1.39	22.62 ± 1.68
2.5	0.1860	0.1012	0.1160	0.731	0.101	11.07 ± 1.30	17.93 ±1.44
3.0	0.1930	0.1105	0.1214	0.680	0.094	9.47 ± 0.47	15.91 ± 1.12

Table 4.5 Physical parameters of PEO(2)-HTAC complexes obtained from light scattering measurements

c_s/c_p	N_s/N_p	$N_{s,b}/N_p$	$N_{s,f}/N_p$	$n_{s,b}$
0.1	191	132	59	~1
0.5	953	408	545	5
1.0	1906	682	1224	9
1.75	3335	1666	1669	22
2.5	4765	1393	3372	19
3.0	5718	1296	4422	17

As evident in Table 4.6, and further exhibited in Figures 4.27 and 4.28, maxima in $R_{h,f}$ and $R_{h,\eta}$ at the maximum binding point at c_s/c_p = 1.75 correlated to those observed in $M_{w,com}$ and R_g. The decreases in R_g, $R_{h,f}$, and $R_{h,\eta}$ at large c_s/c_p presumably appeared because excess added surfactant results in screening of electrostatic interactions between bound micelles and therefore, chain contraction occurred. Note that the apparent hydrodynamic radii, $R_{h,f}$ and $R_{h,\eta}$ obtained by dynamic light scattering and viscometry at finite concentration were not expected to be numerically accurate, because they will be strongly influenced by the effect of intermolecular electrostatic interactions on translational diffusion coefficient and viscosity.

To our knowledge, only one previous study (Gilyani *et al.*, 1985) has utilized a similar combination of light scattering, with the refractive index increment measured at constant chemical potential, and evaluation of the preferential binding of surfactant to determine the molecular weight of polymer surfactant complexes. These authors (Gilyani *et al.*, 1985) investigated the complex formation between poly(vinylpyrrolidone) (PVP) and SDS in 0.1 M $NaNO_3$, and found only unipolymer complex formation occurs up to maximum binding, at which point

essentially all of the surfactants are bound to the polymer, viz. 0.39 mole SDS per mole vinyl- pyrrolidone. In further contrast to our results for the HTAC/PEO system without added salt, SDS/PVP in 0.1 M $NaNO_3$ exhibits a minimum in viscosity, and a minimum in radius of gyration, on addition of surfactant. The lower binding capacity observed in our studies for HTAC with PEO, compared to PVP/SDS/0.1 M $NaNO_3$, is consistent with previous studies, which indicates that the maximum binding ratio increases with addition of inorganic salt. For example, Cabane and Duplessix (1982) observed that the binding ratio of SDS to EO is 0.25 mol SDS per mol EO at zero salt. The small binding ratio of HTAC to EO at zero salt (0.12), compared to that of SDS to EO (0.25) is further consistent with expectation that the binding of cationic surfactant to uncharged polymers is weaker than that of anionic surfactants.

Table 4.6 Variation of $M_{w,com}$, R_g, $R_{h,f}$, and $R_{h,\eta}$ with addition of HTAC

c_s/c_p	$M_{w,com}$ x 10^{-5} (g/mol)	Polydispersity (μ_2/Γ^2)	R_g (nm)	$R_{h,f}$ (nm)	$R_{h,\eta}$ (nm)
0	6.08 ± 0.13	0.47 ± 0.01	86.8 ± 3.2	40.4 ± 3.0	35.7 ± 0.2
0.1	6.54 ±0.20	0.50 ± 0.01	86.9 ± 5.3	56.9 ± 3.8	34.9 ± 0.4
0.5	8.06 ± 0.31	0.59 ± 0.02	95.1 ± 4.9	60.8 ± 3.6	37.4 ± 1.1
1.0	9.24 ± 0.50	0.67 ± 0.01	106.7 ± 7.1	73.6 ± 1.7	41.1 ± 1.5
1.75	22.62 ± 3.68	0.71 ± 0.02	169.8 ± 6.4	81.4 ± 0.4	47.0 ± 3.0
2.5	17.93 ± 1.44	0.69 ± 0.01	151.4 ± 9.1	60.0 ± 4.0	45.1 ± 1.8
3.0	15.91 ± 1.12	0.66 ± 0.02	148.3 ± 1.8	58.0 ± 1.3	44.4 ± 2.0

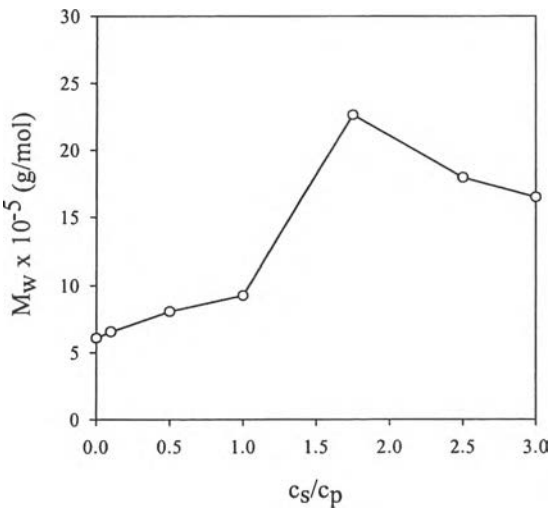

Figure 4.27 Molecular weight of PEO(2)-HTAC complex as a function of surfactant to polymer concentration ratio in ternary solution at 30°C.

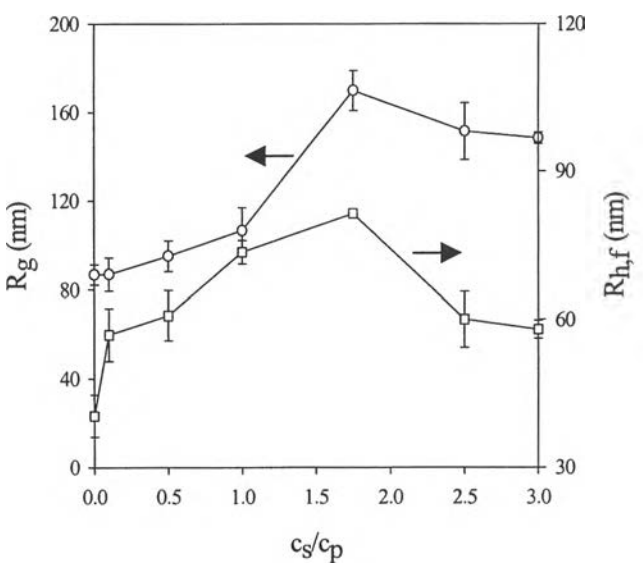

Figure 4.28 Radius of gyration and apparent hydrodynamic radius as a function of HTAC to PEO concentration ratio for PEO(2)-HTAC complex.

Thus, the comparison between our data and that in the PVP/SDS system supports the idea that in salt-free solutions of nonionic polymers, the lower binding capacity leads to a tendency that polymer chains share micelles, when forming complexes with charged surfactants.

Valstar *et al.* (2000) determined that multichain complexes form between SDS and serum albumen, based on light scattering data interpreted via equation (3.27). However, they further reported that the number of protein chains decreases towards unity as the dialysis time increases. No such effect was observed in our study. Also, Greener *et al.* (1987) observed a maximum in viscosity of alkali-processed gelatin on titration with SDS, interpreted as due to cross-linking of gelatin chains by SDS micelles. Finally, a study of complex formation between cetyltrimethylammonium bromide (CTAB) micelles and polyacrylic acid (PAA) at low pH reported that maximum binding occurs when the CTAB/acrylic acid mole ratio = 1.0, at which point no free micelles are present (Fundin *et al.*, 1997). At higher CTAB content, free micelles appear, as evidenced by the appearance of a fast mode in dynamic light scattering analysis, and R_g decreases, due to electrostatic screening. In the CTAB/PAA system, significant ionization of PAA occurs on addition of surfactant, hence the higher binding affinity is likely due to the fact that electrostatic interactions between bound surfactant and acrylate monomer play an important role in stabilizing complex formation.

It is interesting to discuss our observations in light of recent theoretical treatments of the viscosity of a dilute solution of strongly-charged polyions (Cohen *et al.*, 1988; Jiang and Han, 2000). Cohen *et al.* (1988) derived the specific viscosity in the strong coupling limit, omitting numerical prefactors as,

$$\eta_{sp} \approx \frac{R_h l_B^2 c_{po}^2 Z_p^2}{\kappa^3}, \tag{4.3}$$

where R_h is the hydrodynamic radius of the polyion, c_{po} is the polyion concentration in moles/L = c_p'/M_p, where c_p' is the polyion concentration in g/L, and M_p is the polyion molecular weight, Z_p is the net charge on the polyion, and κ is the Debye length, given, for monovalent counterions, by

$$\kappa^2 = 4\pi l_B(c_{po}Z_p + 2c_{salt}), \tag{4.4}$$

where c_{salt} is the concentration of added salt, and $l_B = e^2/\varepsilon_0 k_B T$ is the Bjerrum length, ε_0 is the dielectric constant of the solvent, k_B is Boltzmann's constant, and T is the absolute temperature. Adapting equation (4.4) to our present system, viz. a polymer/micelle complex in equilibrium with free surfactant micelles, we equate $c_p' = c_p(1+D')$, and $M_p = M_w(1+D')$, where D' is the amount of bound surfactant, and the net charge on the PEO/HTAC complex, $Z_p = D'M_w/M_s$, where M_s is the molecular weight of the surfactant. We can further express that,

$$\kappa^2 = 4\pi l_B(c_{po}\alpha_p Z_p + c_{mo}\alpha_m Z_m), \tag{4.5}$$

where $c_{po} = c_p'/M_p = c_p'/M_p = c_p/M_w$, and $c_{mo} = (c_s - c_pD')/M_m$ is the molar concentration of free surfactant micelles, with c_s the total concentration of surfactant, $M_m = M_sZ_m$, where Z_m is the net charge on the micelle, and α_p and α_m referred to the fraction of dissociated counterions for polymer-micelle complex and free micelles, respectively. With these substitutions, a scaling relation for the dependence of η_{sp} on R_h, D' and the ratios c_s/c_p and α_m/α_p was obtained as,

$$\eta_{sp} \approx \frac{R_h c_p^{0.5} \alpha_m^{0.5} (D')^2}{M_s^{0.5} (c_s/c_p)^{1.5} (\alpha_m/\alpha_p)^2}. \tag{4.6}$$

Since α_m, c_p, and M_s are fixed, we may write:

$$\eta_{sp} = \frac{KR_h (D')^2}{(c_s/c_p)^{1.5} (\alpha_m/\alpha_p)^2}, \tag{4.7}$$

where K is a numerical constant. Using our experimentally determined values of R_h and D' (see Tables 4.2 and 4.4), it was found that equation (4.7) indeed predicts a maximum in viscosity, which coincides with that observed at $c_s/c_p = 1.75$. However, to quantitatively match the observed change in viscosity, which increases from $\eta_{sp} \sim$

0.4 at $c_s/c_p = 0.5$, to $\eta_{sp} \sim 0.6$ at $c_s/c_p = 1.75$, and then decreases to $\eta_{sp} \sim 0.5$ at $c_s/c_p = 3.0$, it is necessary, in equation (4.7), to allow that α_m/α_p varies with change in the surfactant to polymer concentration ratio, c_s/c_p. In fact, an increase in α_m/α_p from around 0.5 at small c_s/c_p to approximately unity at maximum binding was reported by Fundin *et al.* (1997), in their study of complexes formed between CTAB and poly(acrylic acid), i.e. at low c_s/c_p, counterion condensation on bound micelles is substantially diminished, and increases to a level comparable to that of free micelles at maximum micelle binding, where it levels off. Hence, if we assume $\alpha_m/\alpha_p = 1.0$ at $c_s/c_p = 1.75$, then from equation (4.7), we deduced α_m/α_p increases from approximately 0.6 at $c_s/c_p = 0.5$, to unity at maximum binding, and then decreases again to approximately 0.48 at $c_s/c_p = 3.0$. It seems likely that the putative decrease in α_m/α_p above maximum binding is erroneous, perhaps signaling a breakdown of the strong coupling approximation, or a crossover from dilute solution to semi-dilute solution behavior, where the theory no longer applies.

4.3.6.2 PEO-HTAC Complex in 0.1 M KNO_3 Solution

Figure 4.29 indicates the Zimm plot for the ternary system of PEO-HTAC complex in 0.1 M KNO_3 solution at constant ratio, $c_s/c_p = 1.75$. The weight-average molecular weight of PEO in the complex, M_w, was determined via equations (3.28) using different dn/dc values. The values for $(dn/dc_p)_{\mu s}$, $(dn/dc_p)_{cs}$, and $(dn/dc_s)c_p$ for the PEO-HTAC complex in salt solution are shown in Table 4.7. The corresponding plots for dn/dc measurement are shown in Appendix (3.5.4). The goal of this work is to contrast the structures of PEO-HTAC complex in the presence and absence of salt. Table 4.7 compares the results of static light scattering from PEO-HTAC complexes in 0.1 M KNO_3 solution versus corresponding values in water at the same c_s/c_p ratio. As shown in Table 4.7, the preferential binding (D') of HTAC to PEO increases from 0.87 to 1.64 (g of HTAC per g of PEO) by adding salt, viz. 0.12 mol HTAC per mol EO increases to 0.23 mol HTAC per mol EO. From the molecular weight data, it was deduced that addition of salt leads to a reduction in formation of multichain aggregates, since the average number of PEO chains in the complex is reduced from 2.0 to essentially 1.18, and thus, the molecular weight of complex in salt solution is significantly lower than that in the free-salt solution. This

result appears to be consistent with the conductivity measurements, which shows that the cac of PEO-HTAC complex in 0.1 M KNO_3 solution (0.35 mM) is smaller than in water (0.56 mM), indicating that the polymer-bound micelles are more stable in salt solution than without salt. Therefore, we deduced that the driving force for PEO chains to share HTAC micelles is that this reduces electrostatic repulsions between surfactant headgroups, and increases the stability of bound micelles at low ionic strength.

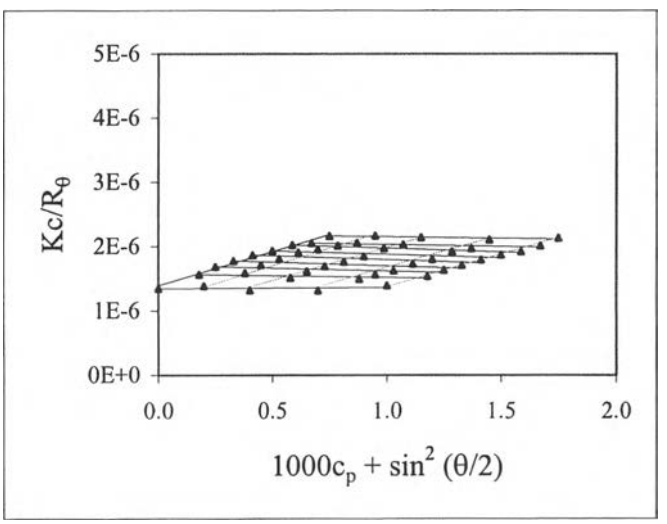

Figure 4.29 Zimm plot for PEO-HTAC complex solution in 0.1 M KNO_3 solution at 30°C, at the maximum binding point (c_s/c_p = 1.75). The lines are drawn by least square fit method.

The R_g for the free PEO chain in the presence of salt was determined to be 68 ± 2.0 nm which was smaller than that observed in water (86.8 ± 3.2 nm). The shrinkage of R_g is consistent with the decrease of η_{sp} and R_h (82.5 nm to 38.0 nm) and reflects the change in chain conformation due to disruption of the structure of water solvation by adding salt. Another interesting feature in Table 4.7 is that the R_g of the PEO-HTAC complex in salt solution is substantially smaller than that of the complex in water, although the $M_{w,com}$ are comparable, because the dissociation of multi-chain complexes is counteracted by an increase in the binding ratio of HTAC to PEO.

Table 4.7 The comparative study of PEO-HTAC complex in aqueous solution and in the presence of 0.1 M KNO_3 solution at the maximum binding point

Physical Parameters	PEO-HTAC complex in water	PEO-HTAC complex in 0.1 M KNO_3 solution
$(dn/dc_p)_{\mu s}$	0.1880 ± 0.004	0.2706 ± 0.002
$(dn/dc_p)_{cs}$	0.1002 ± 0.003	0.1012 ± 0.004
$(dn/dc_s)c_p$	0.1005 ± 0.004	0.1035 ± 0.001
D'	0.87	1.64
$M_w \times 10^{-5}$ (g/mol)	12.07 ± 1.39	7.04 ± 0.13
$M_{w,com} \times 10^{-5}$ (g/mol)	22.62 ± 1.68	18.89 ± 1.06
R_g (nm)	169.8 ± 6.4	75.4 ± 4.4
R_h (nm)	82.5 ± 5.2	38.0 ± 2.4
# of PEO chain	2.0 ± 0.3	1.18 ± 0.02
$N_{s,b}/N_p$	1670	3080

Moreover, R_g of the former is only slightly larger than that of the free PEO chain in salt solution, although the molecular weight of the complex is three times larger. The large decrease in R_g of the PEO-HTAC complex in 0.1 M KNO_3 reflects both screening of electrostatic repulsions and disentanglement of the polymer chains in the complex. The small Rg values of the complex in salt solution

suggest further that the binding of micelles in unipolymer complexes may be accompanied by a contraction of the PEO chain. Finally, we noted that the large decrease in the volume of the chain (R_g^3 decreased by a factor of 11) on adding salt, relative to the fact that $M_{w,com}$ changes very little, has to be reconciled with the observation in viscosity data that the viscosity of the solution near maximum binging decreases by only about 20%. This suggests that the multi-chain aggregates are present as small quantities of large clusters, as indeed observed in the experiments on oppositely-charged polymers and surfactants (Fundin *et al.*, 1996; Lance-Gomez and Ward, 1986). Such clusters contribute little to the viscosity, but have a large effect on the z-average R_g^2.

The number of bound HTAC molecules per PEO chain ($N_{s,b}/N_p$) was calculated through $N_{s,b}/N_p = D'M_{w,PEO}/M_{HTAC}$, where $M_{w,PEO}$ is the molecular weight of PEO in salt solution (599,000 g/mol; the graph is shown in Appendix) and M_{HTAC} is the molecular weight of HTAC (319 g/mol). It was observed that the number of bound HTAC molecules per chain is increased from 50% to 94% (the total number of HTAC molecules per PEO in salt solution = 3290). The increase binding affinity of HTAC to PEO is observed when salt is added due to the reduced electrostatic repulsions between the surfactant headgroups. Our results may be compared with those of Cabane and Duplessix (1982), who reported the binding ratio of 0.25 mol SDS per mol EO without added salt, which increases to 0.85 mol SDS per mol EO at 0.4 ionic strength. Shirahama (1974) and Cabane (1977) also observed in PEO-SDS system that the binding ratio is higher in salt solution than that observed in salt-free systems, viz., ~ 0.2 to 0.4 mol SDS per mol EO, determined by surface tension method. In the case of PVP-SDS system (Murata and Arai, 1973), addition of 0.1 M NaCl increases the ratio to 0.9 mol SDS from the 0.3 mol SDS per mol of vinyl pyrrolidone observed in water. Again, the complex formation between PVP and SDS in 0.1 M $NaNO_3$ (Norwood *et al.*, 1998) indicated that all surfactants are bound to the polymer (0.39 mol SDS per mol vinyl pyrrolidone). It is clear to confirm that the weak binding affinity of surfactant to polymer enhances the tendency of polymer chains to share micelles, when forming complexes between nonionic polymers and charged surfactants in salt-free aqueous solution. To our knowledge, two previous studies of complex formation between

oppositely-charged polymers and surfactants exist (Fundin *et al.*, 1996; Lance-Gomez and Ward, 1986). The former one, involving Polystyrene sulfonate (PSS) and CTAB, found that multichain complexation is enhanced by salt, and the latter, involving SDS and poly(*N,N,N*-trimethylammonio) ethyl acrylate (PCMA) found that addition of salt diminishes the formation of multichain complexes. The difference is attributed to the existence of a hydrophobic driving force or complex formation in the former, whereas electrostatic interactions are the driving force in the latter. In the latter system it is further observed that the stability of the bound micelles is increased in the presence of salt, as evidenced by a decrease in the cac. The formation of multi-chain complexes is associated with a decrease in the stability of bound micelles.

To confirm the occurrence of interpolymer complex in the ternary PEO-HTAC solution in the absence of salt, the particle size distribution (PSD) was presented by dynamic light scattering. Figure 4.30 compares the PSD for a solution containing 0.1 g/100 mL PEO in water and in the presence of salt. A single peak is observed, with the characteristic of a diffusion mode, i.e. the measured hydrodynamic diameter is independent of the scattering angle. In water, the PSD has a mean hydrodynamic radius, R_h = 42 nm, which reduces to R_h = 35 nm in 0.1 M KNO_3. This result agrees well with the shrinkage of R_g in the presence of salt.

Figure 4.31 shows the PSD for the ternary PEO-HTAC solution at a constant concentration ratio, c_s/c_p = 1.75, in the presence and absence of salt, respectively. The PSD in 0.1 M KNO_3 is, in fact, very similar to that of the PEO itself (Figure 4.30), whereas in the absence of salt, the PSD has a very broad distribution, with a prominent high molecular weight "tail", which can be ascribed to the presence of large multichain aggregates. Addition of salt leads to a reduction in the mean size of the complex from R_h = 82.5 nm to 38 nm, in good agreement with the R_g values, which also decreases by a factor of two on adding salt.

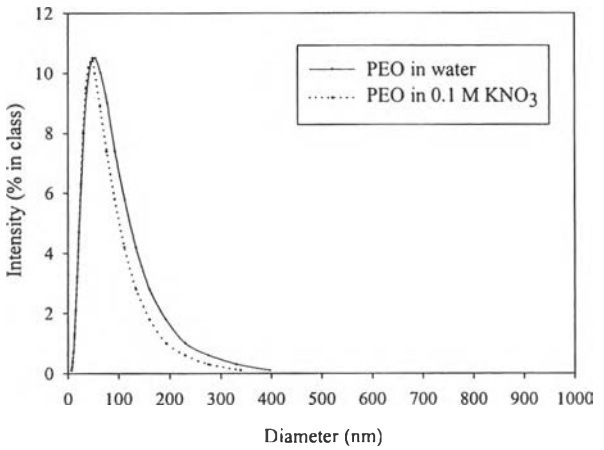

Figure 4.30 The particle size distribution of PEO solution. The solid line represents the PEO in water and the dashed line corresponds to the PEO in 0.1 M KNO_3 solution.

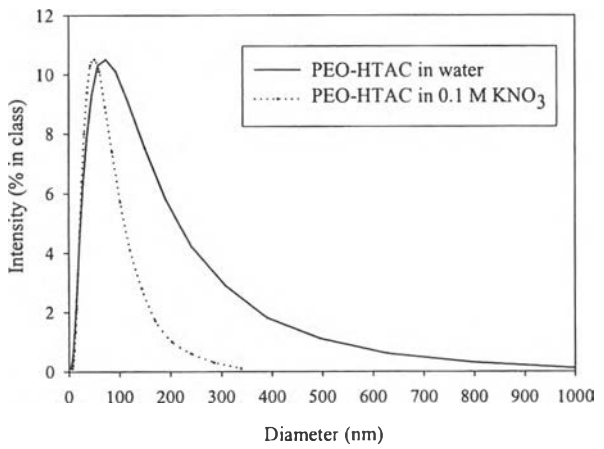

Figure 4.31 The particle size distribution of PEO-HTAC solution at HTAC/PEO ratio = 1.75 (maximum binding point).

4.4 Viscoelastic Properties of PEO in Water

To investigate the viscoelastic properties of PEO, dynamic oscillatory measurements were performed at PEO concentrations of 4 g/dL and 8 g/dL, and the temperature was varied from 10°C to 50°C.

Figures 4.32 and 4.33 show the frequency dependence of the storage modulus (G'), the loss modulus (G"), and the complex viscosity (η^*) of PEO in water for 4 g/dL and 8 g/dL at 30°C in a double logarithmic plot. The viscosity profiles show a Newtonian plateau at low frequencies, followed by shear-thinning behavior at high frequencies (8 g/dL). The zero shear viscosity (η_o^*) was obtained in the Newtonian plateau region. As expected, the shear-thinning behavior is more prominent at higher PEO concentration. The slopes of log G' and log G" versus log ω plots approach the values of 2 and 1, respectively, indicating viscoelastic (Rouse-like) behavior (Ferry, 1980). The loss modulus G" is always higher than the storage modulus G' over the entire frequency range. This indicates predominantly viscous behavior of polymer with relatively low storage of energy during the polymer deformation. A crossover in G' and G" is observed at high frequency ($\omega_c \sim 100\ s^{-1}$) for 8 g/dL PEO concentration.

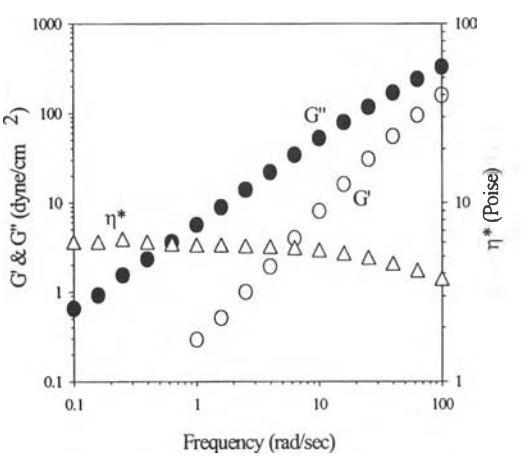

Figure 4.32 Double logarithmic plot of the storage modulus (G'), the loss modulus (G"), and the complex viscosity (η^*) as a function of frequency (ω) for PEO 4 g/dL at 30°C.

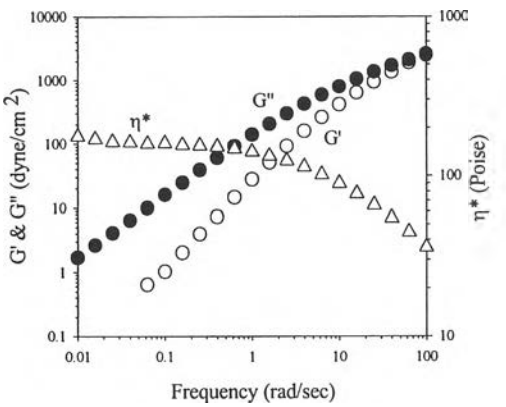

Figure 4.33 Double logarithmic plot of the storage modulus G', the loss modulus G", and the complex viscosity η* as a function of frequency ω for PEO 8 g/dL at 30°C.

4.4.1 Salt Effect

The effect of salt (KNO_3) on the rheology of PEO solutions was also investigated. In Figure 4.34, the storage modulus G', the loss modulus G", and the complex viscosity η* are plotted as a function of frequency for PEO (4 g/dL) in both water and in 0.1 M KNO_3 solution.

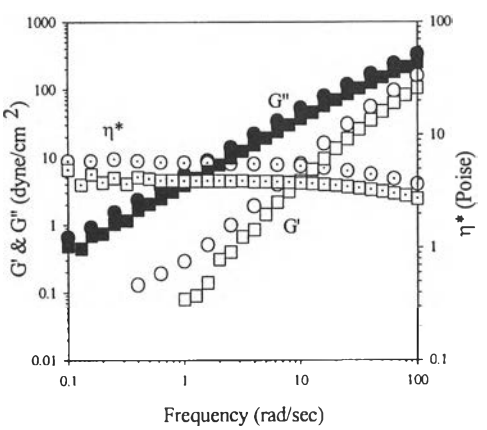

Figure 4.34 Double logarithmic plot of G', G", and η* as a function of ω for 4 g/dL PEO in water (open, closed, and dotted circles) and in 0.1 M KNO_3 solution (open, closed, and dotted squares) at 30°C.

The viscosity and dynamic moduli slightly decrease in the presence of salt. This result is attributed to the fact that added salt reduces the hydrophilic stabilization of the polymer backbone, and hence reduces the size of the PEO chain, i.e. the effective solvent quality becomes poorer.

4.4.2 Temperature Effect

Figures 4.35 and 4.36 show the reduced storage (G_R') and loss moduli (G_R") as a function of reduced frequency (ω_R) for PEO (4 g/dL) and (8 g/dL) at different temperatures. The temperature was varied from 10°C to 50°C. The reduced parameters were calculated according to equations (3.48), (3.49), and (3.50), respectively, viz. $G_R' = G'M/cRT$; $G_R'' = (G''- \omega\eta_s)_R = (G''- \omega\eta_s)\, M/cRT$; and $\omega_R = \omega(\eta_0 - \eta_s)\, M/cRT$, to construct the master curve.

As shown in Figures 4.35 and 4.36, the slope of the log G_R' versus log ω_R plot is approximately 2 and log G_R'' is proportional to log ω, suggesting that the polymer solution follows the Rouse model dynamics. We observe some scattering of the data, deviating from the scaling behavior in the master curve, which may be experimental error.

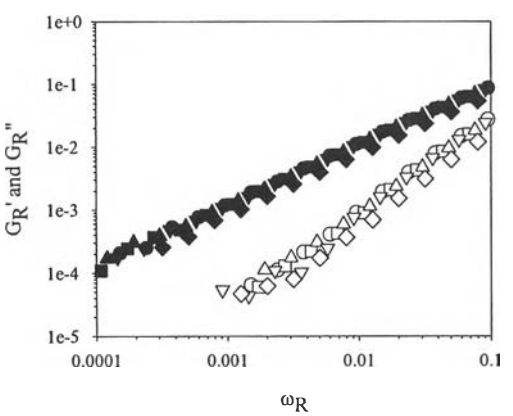

Figure 4.35 Double logarithmic plot of the reduced storage modulus G_R', and the reduced loss modulus G_R'' versus the reduced frequency ω_R for PEO 4 g/dL at different temperatures. (O) 10°C; (□) 20°C; (Δ) 30°C; (∇) 40°C; and (◊) 50°C. The open symbols represent G_R' and the closed symbols refer to G_R''.

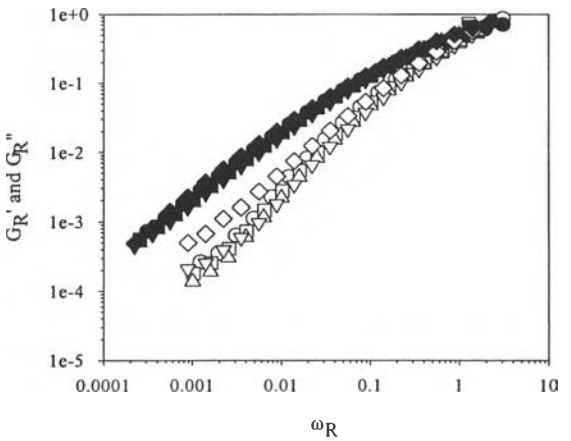

Figure 4.36 Double logarithmic plot of the reduced storage modulus G_R', and the reduced modulus G_R'' versus the reduced frequency ω_R for PEO 8 g/dL at different temperatures. (O) 10°C; (□) 20°C; (Δ) 30°C; (∇) 40°C; and (◊) 50°C.

In Figure 4.36, G_R' seems significantly higher than the master curve at 50°C, compared to the other temperatures. This may reflect some structural change in the polymer, e.g. intermolecular asociation due to the decreased hydrophilicity, which may alter the degree of entanglement of the polymer chain as temperature increases.

The corresponding viscosity versus frequency plots are shown in Figures 4.37 and 4.38. Generally, η^* decreases with increasing temperature because the polarity of the solvent reduces at higher temperatures. The viscosity profiles show more Newtonian behavior at higher temperatures. However, in Figure 4.38, η^* suddenly increases from ~ 150 Ps at 40°C to ~ 200 Ps at 50°C. Noting that at this temperature, time-temperature superposition fails, we speculate again that there may be some kind of structural change, e.g. intermolecular association, which alters the degree of entanglement of the solution with increase of temperature at the higher PEO concentration (8 g/dL).

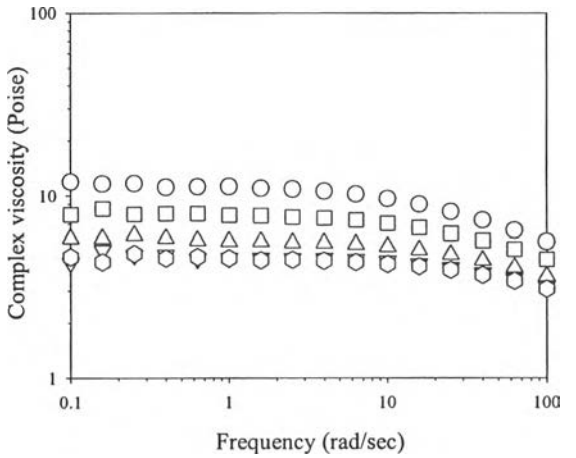

Figure 4.37 The complex viscosity η* versus frequency for PEO 4 g/dL at different temperatures. (O) 10°C; (□) 20°C; (Δ) 30°C; (∇) 40°C; and (◊) 50°C.

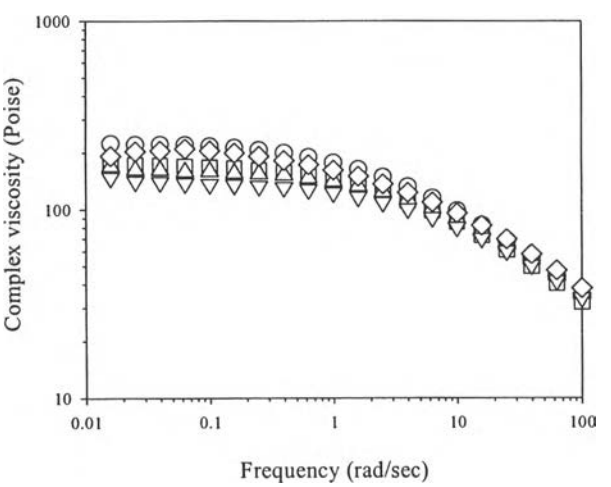

Figure 4.38 The complex viscosity η* versus frequency for PEO 8 g/dL at different temperatures. (O) 10°C; (□) 20°C; (Δ) 30°C; (∇) 40°C; and (◊) 50°C.

4.5 Viscoelastic Properties of HTAC Micelles

Figure 4.39 shows the complex viscosity (η^*) of HTAC solutions as a function of frequency for two different surfactant concentrations, 0.25 M and 0.5 M at T = 30°C (8 g/dL and 16 g/dL HTAC). At these temperatures, the solution behaves as a non-Newtonian shear-thinning fluid. These observations seem consistent with results obtained by Cappelaere *et al.* (1995), who reported that spherical micelles exist in cetyltrimethylammonium bromide (CTAB) solutions from the critical micelle concentration (cmc) up to approximately 0.2-0.3 M, above which long wormy micelles form, as shown in Figure 4.40. Thus, the viscosity exhibits non-Newtonian behavior presumably because the presence of wormy micelles. Surprisingly, although the viscosity is higher at higher concentration, the onset of shear-thinning occurs at lower frequency, which means the viscoelastic relaxation time is longer.

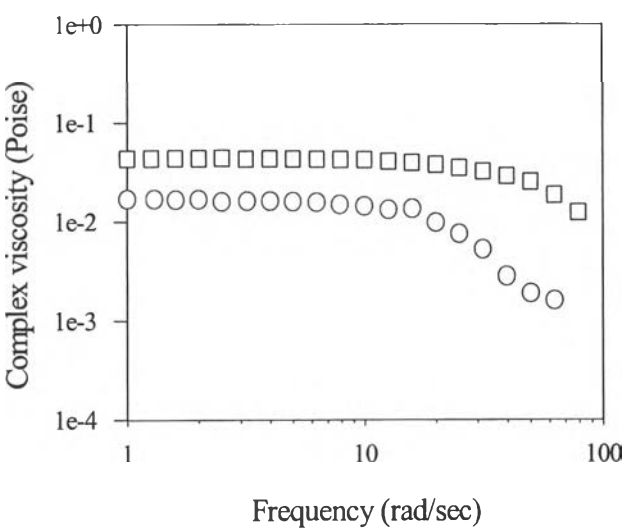

Figure 4.39 The complex viscosity (η^*) as a function of frequency for two different concentrations: 0.25 M (O) and 0.5 M (□) at T = 30°C (8 g/dL and 16 g/dL HTAC).

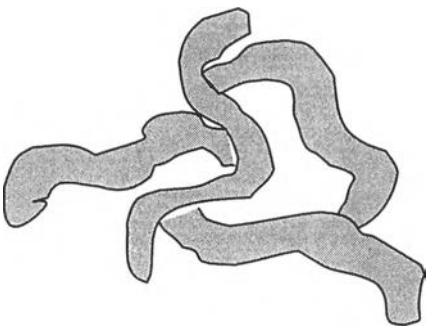

Figure 4.40 The schematic drawing of flexible wormy micelles (Larson, 1999).

Figure 4.41 (A) and (B) show the logarithmic plot of G' and G" versus frequency for a solution of 0.5 M HTAC at different temperatures (10° – 50°C) in dynamic oscillatory measurement. At low frequencies, G' and G" follow the simple Maxwell model behavior (i.e., $G' \propto \omega^2$ and $G'' \propto \omega$) at any experimental temperatures. At high frequencies, G" exhibits a maximum, consistent with the single exponential Maxwell relaxation model. As temperature increases, a clear plateau modulus (G_0) is seen at high temperatures (> 30°C), again consistent with the Maxwell model. In general, a shorter relaxation time is expected to occur on increasing temperature, according to the equation: $\eta_0 = G_0\tau_R$, since it is expected that η_o decreases and G_o increases on increasing temperature. However, surprisingly, in Figure 4.41 the maximum moves to lower frequencies, indicative that a longer relaxation time is observed with increasing temperature. The variation of the complex viscosity (η^*) as a function of frequency (ω) at different temperatures for 5 M HTAB solution is shown in Figure 4.43. As expected, the Newtonian viscosity, η_o, slightly decreases with increasing temperature in the range 10°C - 50°C. However, surprisingly the onset of shear-thinning occurs again at lower frequency for higher temperatures. Applying the Maxwell model to these data, we find that a decrease in plateau modulus (G_0) exceeds the increase of relaxation time (τ_R) as shown in Figure 4.42.

In the scaling theory, the shear modulus (G) is predicted to be proportional to k_BT/ξ^3, where ξ is defined as the diameter of the tube into which the chain reptates. One expects that a slight decrease of ξ as increasing temperature due to both an expansion of the whole micelles and a decrease of persistence length, and therefore

the shear modulus should slightly increase with temperature. However, our data shows that G_0 decreases with increasing temperature as shown in Figure 4.42 and Table 4.8. Similar unusual behavior was found in work of Candau *et al.* (1989), who observed that the shear modulus slightly decreased with temperature. They proposed that the effect is due to a difference between the size of the micellar chain between two successive entanglements and the hydrodynamic length of the chain (L_H).

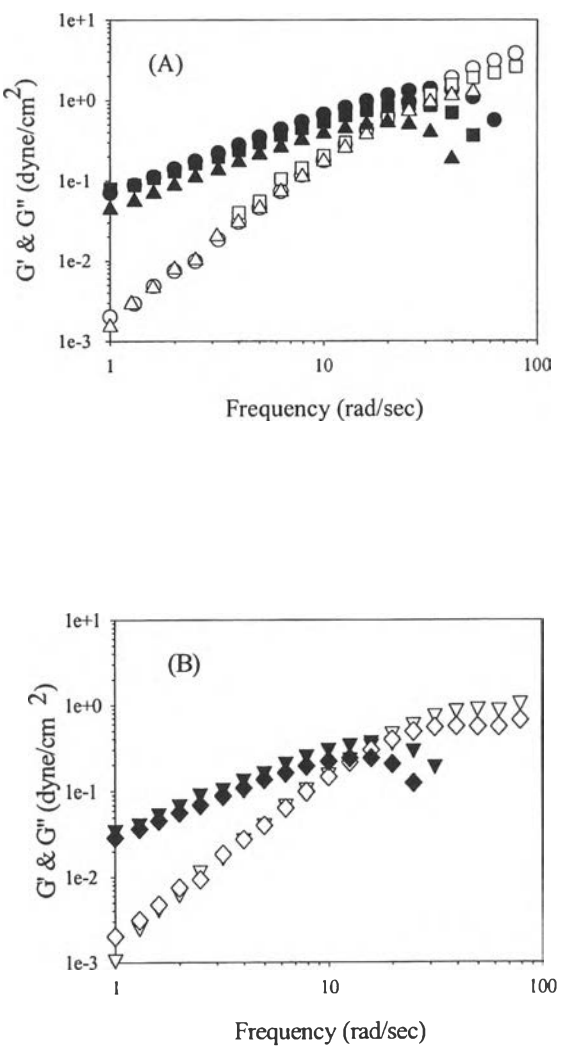

Figure 4.41 Logarithmic plot of the storage modulus G', the loss modulus G" versus frequency for a solution of 0.5 M HTAC (16 g/dL) at different temperatures: (A) 10°C (O); 20°C (□); and 30°C (Δ); (B) 40°C (∇); and 50°C (◊). The open symbols represent G_R' and the closed symbols refer to G_R".

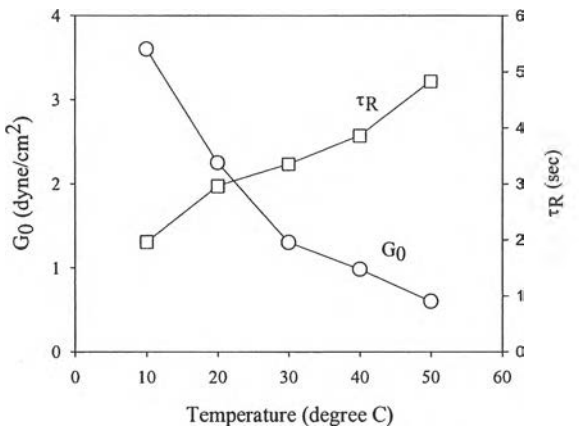

Figure 4.42 The temperature dependence of plateau modulus (G_0) and the stress relaxation time (τ_R).

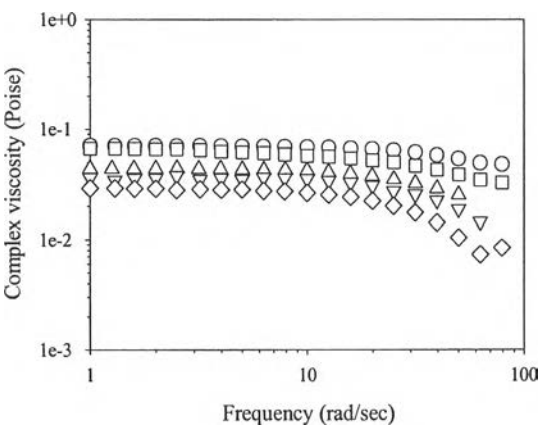

Figure 4.43 The variation of the complex viscosity (η^*) as a function of frequency at different temperatures for 0.5 M HTAC (16 g/dL) solution. (O) 10°C; (□) 20°C; and (Δ) 30°C; (∇) 40°C; and (◊) 50°C.

The extent to which the results deviate from a single exponential relaxation function in the ideal Maxwell model can be represented in the form of a Cole-Cole plot which plots the imaginary part G"(ω) of the shear modulus against the real part G'(ω). Depending on the conditions such as surfactant concentration, salt concentration, and temperature, the Cole-Cole plot of concentrated surfactant

solutions is found to vary from a semicircular shape, characteristic of a single exponential stress relaxation, to a non-semicircular shape, indicative of a non-exponential relaxation at short time scales (Turner and Cates, 1991). Figures 4.44 (A) to (E) indicate the experimental Cole-Cole plots represented in a classical form, i.e. G" (ω) versus G' (ω) for 0.5 M HTAC solution at different temperatures. The dashed lines correspond to the semicircle, representing ideal Maxwell behavior. Note that the distortion from a semicircle into an ellipse occurs because of the differing scales of abscissa and ordinate. As shown in the Figures, the experimental data superpose onto the semicircle at low frequencies, indicating the Maxwellian behavior. The deviation from a semicircular shape is observed at high frequencies at all temperatures. It can be seen that the deviation from single exponential relaxation is similar at high temperature, but slightly larger at low temperature as shown in Table 4.8, which was calculated from the ratio of the diameter of experimental data (solid line in Figure 4.44) to the diameter of fitted semicircle (dashed line in Figure 4.44), together with the values of η_0 and G_0.

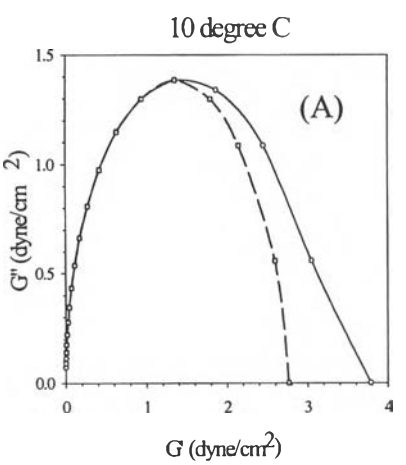

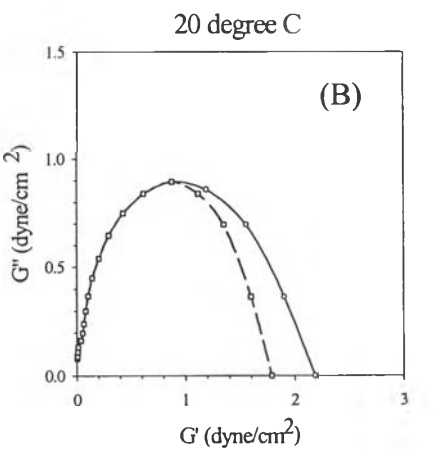

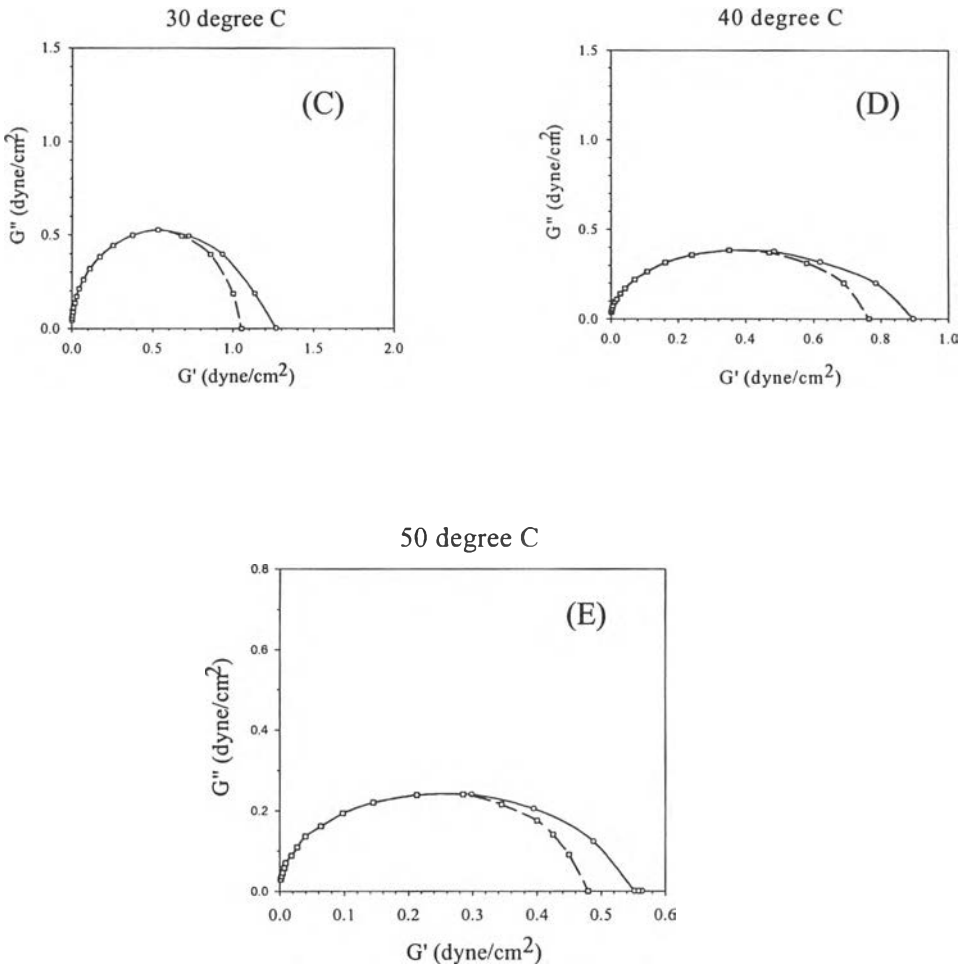

Figure 4.44 The Cole-Cole plot, represented as the loss modulus G" versus the storage modulus G', for 0.5 M HTAC solution at different temperatures. (A) 10°C; (B) 20°C; (C) 30°C; (D) 40°C; (E) 50°C.

The breaking time relaxation τ_b is difficult to measure in concentrated system. Alternatively, it can be able to estimate according to the procedure of Turner and Cates (1991). In their work, the plot of $\mu''(\omega)$ $[G''(\omega)/G_0]$ vs. $\mu'(\omega)$ $[G'(\omega)/G_0]$ was drawn between 0 and 1. G_0 is the plateau modulus, which was obtained by performing linear extrapolation in the Cole-Cole plot (Figure 4.44) to the horizontal axis with slope -1. Then a least-squares fit of a semicircle was performed through the Cole-Cole plot that lies to the maximum of $\mu''(\omega)$. In this way, the center of the

Table 4.8 The deviation from single exponential function, together with the values of G_0 and η_0 at different temperatures

Temperature (°C)	Deviation	η_0 (Poise)	G_0 (dyne/cm^2)
10	1.29	7.05	3.60
20	1.28	6.65	2.25
30	1.24	4.35	1.30
40	1.26	3.78	0.98
50	1.25	2.90	0.60

semicircle lies on the $\mu'(\omega)$ axis and the semicircle pass through 0 and 1. Figure 4.45 shows the experimental Cole-Cole diagram for various temperature (10°C – 50°C) plotted as $\mu''(\omega)$ vs. $\mu'(\omega)$. From this graph, the diameter of the fitted semicircle (DFS) was obtained for each temperature.

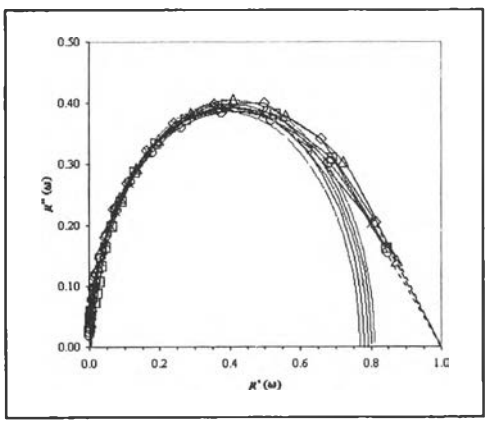

Figure 4.45 Experimental Cole-Cole diagram, plotted as $\mu''(\omega)$ vertical and $\mu'(\omega)$ horizontal for five different temperatures, from inside to outside: 10°C to 50°C.

Figure 4.46 shows the diameter of fitted semicircle (DFS) plotted against $\bar{\zeta}$, which is defined as $\bar{\zeta} = \tau_b/\tau_R$, τ_R is the terminal relaxation time. This figure was obtained by simulation, reprinted from Turner and Cates (1991). From this graph, $\bar{\zeta}$ can be estimated for each temperature by interpolating the plot. Since τ_R was determined according to the equation: $\eta_0 = G_0\tau_R$, and therefore τ_b can be estimated.

Table 4.9 shows the values of DFS, $\bar{\zeta}$, τ_R and τ_b for each temperature. As seen in Table, the values of τ_R and τ_b increase by raising temperature, which is different from the results for the cationic surfactant CTAB in the presence of salt (Cates and Candau, 1990). To understand the origin of these changes in micellar structure requires theory of micelle structure in the presence of electrostatic interaction. Cappelaere *et al.* (1995) proposed that Cates' theory is only applicable for highly concentrated system in the presence of salt. At present, our system cannot be explained by existing theories.

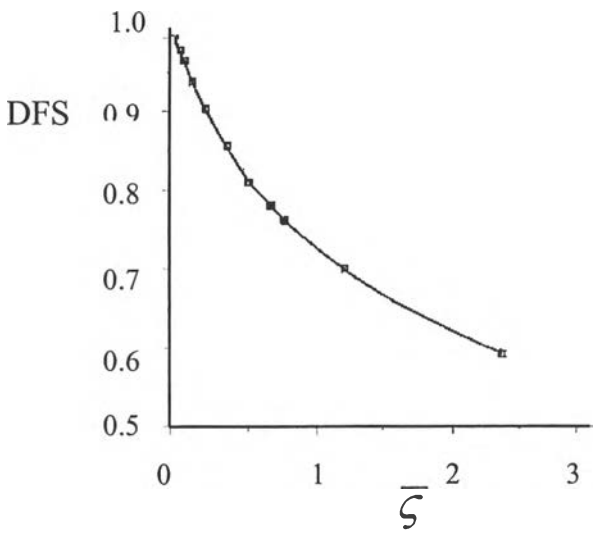

Figure 4.46 Diameter of fitted semicircle (DFS) plotted against $\bar{\zeta}$ (horizontal axis). Numerical points joined by simple interpolation and constrained to pass through (1,0). Reprinted from Turner and Cates, Langmuir, 1991.

Table 4.9 The data of DFS, $\bar{\zeta}$, τ_R and τ_b for different temperatures

T (°C)	DFS	$\bar{\zeta}$	τ_R (S)	τ_b (S)
10	0.77	0.70	1.96	1.37
20	0.79	0.56	2.96	1.66
30	0.81	0.50	3.35	1.67
40	0.78	0.64	3.86	2.47
50	0.80	0.51	4.83	2.47

4.6 Viscoelastic Properties of PEO-HTAC Complex Solutions

4.6.1 PEO-HTAC Complex in Water

To study the viscoelastic properties of PEO-HTAC complex solution, the PEO concentrations were fixed at 4 g/dL and 8 g/dL, and the HTAC concentrations were varied to obtain the constant PEO-HTAC concentration ratios at c_s/c_p = 0.5, 1.0, 1.5, and 2.0. The temperature was varied from 10°C to 50°C.

Figure 4.47 shows the master curve for PEO (4 g/dL)-HTAC (2 g/dL) (c_s/c_p = 0.5) complex in water, plotted as the reduced moduli (G_R' = G'M/cRT; G_R" = (G"- $\omega\eta_s$) M/cRT) versus reduced frequency ($\omega_R = \omega(\eta_0 - \eta_s)$ M/cRT) at different temperatures. At higher temperatures, G_R' and G_R" are higher in PEO-HTAC complex solution than observed in both free PEO and HTAC solutions, presumably because of binding of HTAC micelles to PEO, which invalidates the use of the PEO molecular weight as a scaling parameter.

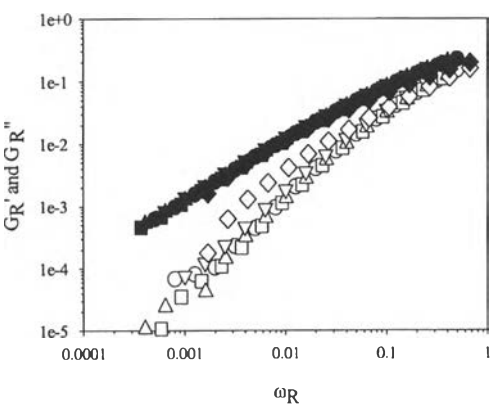

Figure 4.47 The reduced moduli (G_R' and G_R") as a function of reduced frequency (ω_R) for PEO (4 g/dL)-HTAC (2 g/dL) (c_s/c_p = 0.5) at different temperatures: (O) 10°C; (□) 20°C; (Δ) 30°C; (▽) 40°C; and (◊) 50°C. The open symbols refer to G_R' and the closed symbols represent G_R".

Figure 4.48 depicts the frequency dependence of the complex viscosity for PEO-HTAC at c_s/c_p = 0.5 at five different temperatures. The viscosity slightly decreases by changing temperature from 10°C to 20°C, and then gradually

increases by increasing temperature from 20°C to 50°C. This observation is in good agreement with that observed in dilute solution of PEO-HTAC complex. In dilute solution, the PEO-HTAC complex begins to occur at 25°C, determined by light scattering and viscosity. Below 25°C, the viscosity decreases as increasing temperature because of the decrease of solvent quality. Above this temperature, the HTAC micelles bind to PEO, producing a chain expansion due to electrostatic repulsions between bound micelles, resulting in an increase in viscosity with increasing temperature. The interesting feature is that the viscosity dramatically increases about 5 times at 50°C and no Newtonian plateau region is observed at that temperature.

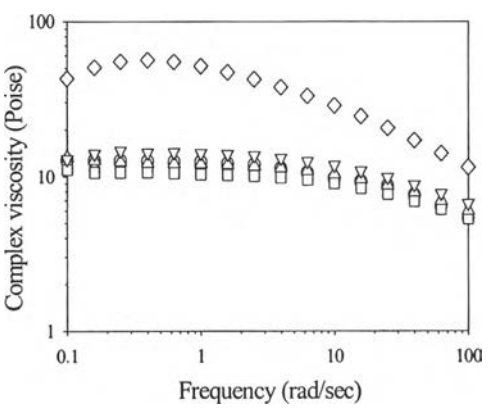

Figure 4.48 The complex viscosity as a function of frequency for PEO-HTAC at c_s/c_p = 0.5 at different temperatures. (PEO concentration: 4 g/dL; HTAC concentration: 2 g/dL). (O) 10°C; (□) 20°C; (Δ) 30°C; (∇) 40°C; and (◊) 50°C.

Figure 4.49 indicates the frequency dependence of storage and loss moduli, plotted in reduced form, for PEO (4 g/dL) and HTAC (6 g/dL) at c_s/c_p = 1.5 at different temperatures. This concentration ratio is near the maximum binding point of HTAC to PEO in dilute aqueous solution (see in section 4.3.1). This means that the PEO chains are saturated with HTAC micelles and therefore a maximum chain expansion occurs at around this concentration region. As shown in Figure, the G_R' and G_R" are slightly higher than those observed at c_s/c_p = 0.5. It is assumed that the

progressive increase of the polymer-surfactant aggregates induces a cross-linking between each other which gives rise to an increase in the modulus. An enormous increase in G_R' and G_R" on addition of surfactant is obvious at 50°C and it indicates the breakdown of time-temperature superposition. At 50°C, the PEO-HTAC complex solution suddenly shows substantially more elastic behavior.

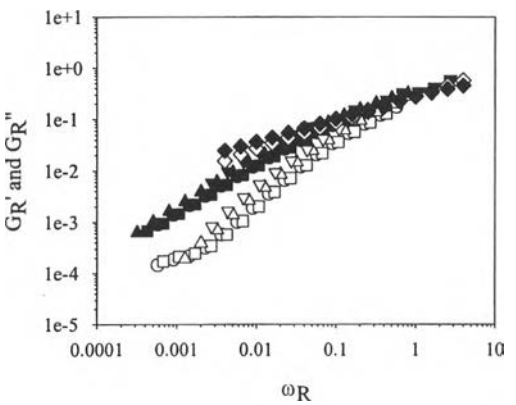

Figure 4.49 The reduced moduli (G_R' and G_R") as a function of reduced frequency (ω_R) for PEO (4 g/dL)-HTAC (6 g/dL) (c_s/c_p = 1.5) at different temperatures. (O) 10°C; (□) 20°C; (Δ) 30°C; (▽) 40°C; and (◊) 50°C. The open symbols refer to G_R' and the closed symbols represent G_R".

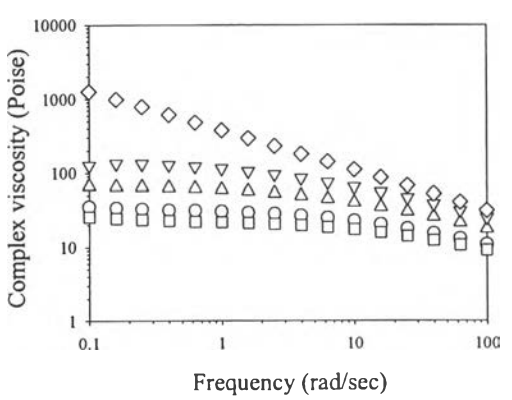

Figure 4.50 Frequency dependence of viscosity at different temperatures for c_s/c_p = 1.5. (PEO concentration: 4 g/dL; HTAC concentration: 6 g/dL). (O) 10°C; (□) 20°C; (Δ) 30°C; (▽) 40°C; and (◊) 50°C.

The viscoelasticity is greatly enhanced when HTAC micelles bind to the PEO, indicated by the increase in complex viscosity above 20°C as shown in Figure 4.50. The complex viscosity (η^*) becomes strongly frequency dependent in an entire range of frequency at 50°C and a lack of zero-shear viscosity (η_0^*) is observed. Brackman (1991) also reported that SDS micelles greatly enhance the viscoelasticity of PEO in aqueous solution, as evidenced by increasingly non-Newtonian behavior.

Figure 4.51 shows a logarithmic plot of reduced storage and loss moduli as a function of reduced frequency for PEO (4 g/dL)-HTAC (8 g/dL) at c_s/c_p = 2.0 at different temperatures. This concentration ratio is beyond the maximum binding point, based on results from viscosity and dynamic light scattering measurements in dilute solution (see in Section 4.3.1). As evident by comparing Figure 4.51 versus Figure 4.49, the moduli values are dramatically lower than observed at c_s/c_p = 1.5.

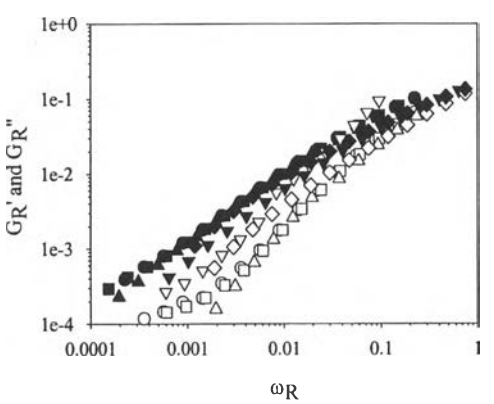

Figure 4.51 Master curve for PEO (4 g/dL)-HTAC (8 g/dL) at c_s/c_p = 2.0 at different temperatures. (O) 10°C; (□) 20°C; (Δ) 30°C; (∇) 40°C; and (◊) 50°C. The open symbols refer to G_R' and the closed symbols represent G_R".

In dilute solution, a decrease in η_{sp} and R_h is observed because of electrostatic screening between the charged particles due to the large amount of counterions. In concentrated solution, however, electrostatic interactions are strongly screened, and it is likely that the decrease in the moduli reflects a breakdown of the

polymer-surfactant aggregates, which reduces the stiffness of PEO-HTAC complex. The corresponding viscosity versus frequency plot is shown in Figure 4.52.

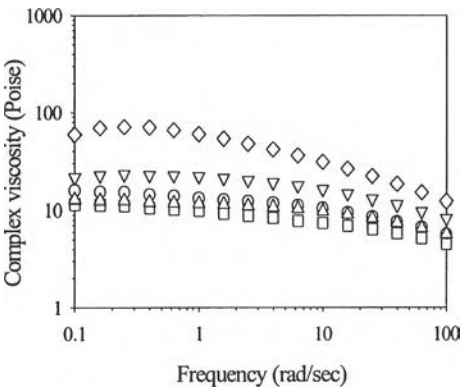

Figure 4.52 The complex viscosity versus frequency for c_s/c_p = 2.0 at different temperatures. (PEO concentration: 4 g/dL; HTAC concentration: 8 g/dL). (O) 10°C; (□) 20°C; (Δ) 30°C; (∇) 40°C; and (◊) 50°C.

The viscosity is reduced an order of magnitude by increasing the amount of surfactant beyond the maximum binding point. Again, this behavior is thought to originate from a breakdown of the polymer-surfactant complex, resulting in a smaller size of the PEO-HTAC aggregates. These observations agree with those of Cabane and Duplessix (1985), who found that the binding of SDS micelles onto PEO in dilute solution becomes weaker when the SDS concentration increases above the saturation point. Figure 4.53 indicates a semi-logarithmic plot of complex viscosity (η^*) versus temperature for different HTAC concentrations, including the free PEO solution (PEO concentration is 4 g/dL). The frequency was fixed at 0.25 rad/sec. In pure PEO solution, the complex viscosity decreases with increasing temperature because of the poorer solvent quality. On addition of surfactant, the viscosity increases very rapidly due to the formation of PEO-HTAC complex and the increment of the degree of entanglement. The increase in viscosity is most pronounced at c_s/c_p = 1.5 which is near the maximum binding of HTAC to PEO. Beyond that concentration ratio, a decrease in complex viscosity is observed because of the partial breakdown of the PEO-HTAC complex.

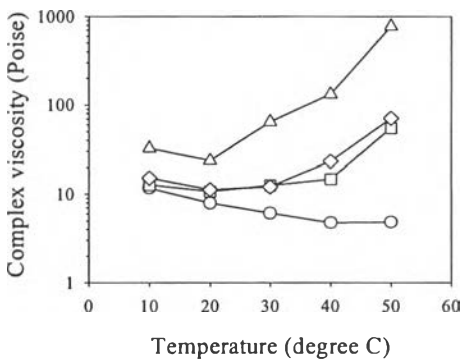

Figure 4.53 The complex viscosity at $\omega = 0.25$ rad/s as a function of temperature for different HTAC concentration. (O) free PEO (4 g/dL) solution, (□) PEO 4 g/dL + HTAC 2 g/dL; (Δ) PEO 4 g/dL + HTAC 6 g/dL; and (◊) PEO 4 g/dL + HTAC 8 g/dL.

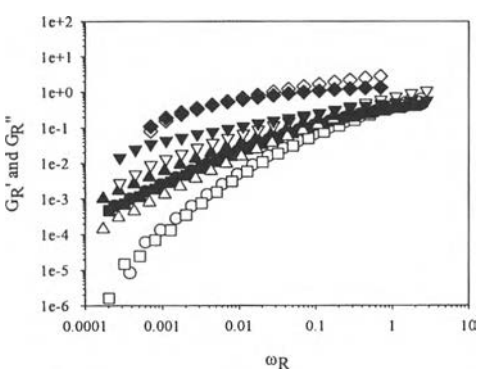

Figure 4.54 The reduced storage and loss moduli (G_R' and G_R") as a function of reduced frequency (ω_R) for PEO-HTAC complex at $c_s/c_p = 1.5$ (PEO concentration: 8 g/dL; HTAC concentration: 12 g/dL). (O) 10°C; (□) 20°C; (Δ) 30°C; (▽) 40°C; and (◊) 50°C. The open symbols refer to G_R' and the closed symbols represent G_R".

Figure 4.54 depicts the master curve for PEO (8 g/dL)-HTAC (12 g/dL) complex near the maximum binding point ($c_s/c_p = 1.5$). The corresponding graphs for the other concentration ratios ($c_s/c_p = 1.0$, and $c_s/c_p = 2.0$) are shown in the Appendices (6.1.4 and 6.1.6). It is clearly seen that the reduced moduli greatly

increase above 20°C when compared to the same concentration ratio with lower PEO concentration (PEO concentration = 4 g/dL-HTAC concentration = 6 g/dL). The breakdown of time-temperature superposition appears even at 30°C. The PEO-HTAC solution shows enhanced elastic behavior compared to the lower concentration, indicative that the degree of entanglement (network formation) increases with increasing PEO concentration and temperature.

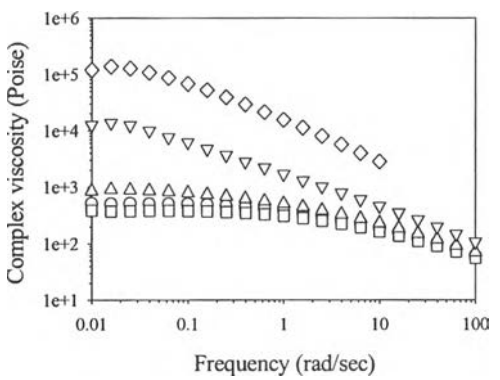

Figure 4.55 The logarithmic plot of complex viscosity as a function of frequency at different temperatures. PEO concentration = 8 g/dL-HTAC concentration = 12 g/dL at c_s/c_p = 1.5. (O) 10°C; (□) 20°C; (Δ) 30°C; (∇) 40°C; and (◊) 50°C.

Figure 4.55 indicates the logarithmic plot of complex viscosity (η^*) as a function of frequency (ω) for PEO-HTAC complex at c_s/c_p = 1.5 at different temperatures. The frequency was fixed at 0.25 rad/sec. The PEO concentration was 8 g/dL and the HTAC concentration was 12 g/dL, respectively. The complex viscosity slightly decreases on increasing temperature from 10°C to 20°C. At that temperature range, there is no complexation between PEO and HTAC in dilute aqueous solution, as indicated by viscosity and dynamic light scattering measurements. In contrast, the complex viscosity increases by 2.5 orders of magnitude and no zero-shear viscosity is found when the temperature rises from 30°C to 50°C, reflecting the formation of temperature-induced structure at higher polymer concentration. Figure 4.56 indicates the semi-logarithmic plot of complex viscosity (η^*) versus temperature for different HTAC concentrations, including the free PEO solution (PEO concentration is 8

g/dL). The behavior is similar to that at lower PEO concentration in Figure 4.53, except that the viscosities are larger at higher PEO concentration.

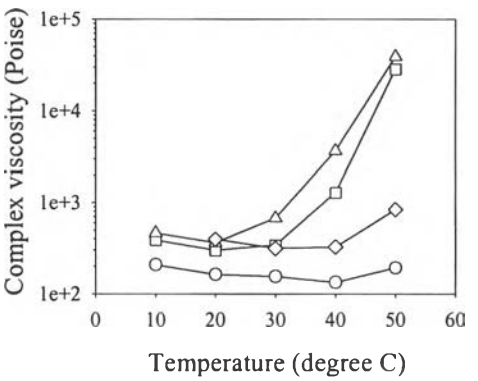

Figure 4.56 The temperature dependence of complex viscosity for different HTAC concentrations: (O) free PEO (8 g/dL) solution, (□) PEO 8 g/dL + HTAC 8 g/dL; (Δ) PEO 8 g/dL + HTAC 12 g/dL; and (◊) PEO 8 g/dL + HTAC 16 g/dL.

4.6.2 PEO-HTAC complex in 0.1 M KNO_3 Solution

Figure 4.57 indicates the frequency dependence of storage and loss moduli, plotted in a reduced form, for PEO (4 g/dL) and HTAC (6 g/dL) in 0.1 M KNO_3 solution at c_s/c_p = 1.5 at different temperatures. The characteristic features of the plot are the same in the presence of salt as those reported above in water, but the reduced moduli slightly decrease with added salt due to increased screening of electrostatic repulsions between the bound micelles and also due to the disentanglement of the polymer chains in the complex. Here, we recall that light scattering analysis in dilute solutions shows multi-chain complexes form in water, whereas predominantly single-chain complexes form in 0.1 M KNO_3. At higher temperature (40°C and 50°C), the reduced moduli deviate from the scaling behavior due to the enhanced formation of PEO-HTAC complex. Also shown in Figure 4.58, the concentration dependence of the complex viscosity in the PEO-HTAC solution on addition of salt is similar to that in water.

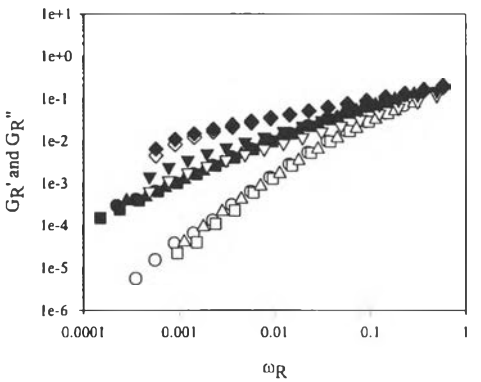

Figure 4.57 The reduced storage (G_R') and loss moduli (G_R'') plotted as a function of reduced frequency (ω_R) for PEO (4 g/dL) and HTAC (6 g/dL) in 0.1 M KNO_3 solution at $c_s/c_p = 1.5$ at different temperatures.

However, the complex viscosity reduces from 1000 poise to 300 poise at 50°C on adding salt. The complex viscosity increases above 20°C, which is consistent with the study of PEO-HTAC system in dilute solution due to the formation of polymer-surfactant complex. The viscosity increases 1.5 orders of magnitude when the temperature changes from 10°C to 50°C and the frequency dependence complex viscosity is also observed at 50°C.

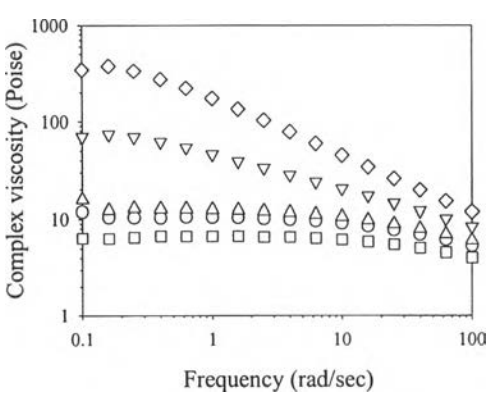

Figure 4.58 The frequency dependence of complex viscosity for PEO (4 g/dL)-HTAC (6 g/dL) in 0.1 M KNO_3 solution at $c_s/c_p = 1.5$ for five different temperatures (O) 10°C; (□) 20°C; (Δ) 30°C; (▽) 40°C; and (◊) 50°C.

4.7 Investigation of HPC-CADG Interaction

In this section, the interaction between nonionic cellulose polymer (HPC) with amphoteric surfactant (CADG) will be presented. To our knowledge, there is no evidence for the existence of a binding interaction between nonionic polymer and amphoteric surfactant. For this reason, we investigated the formation of a neutral polymer with amphoteric surfactant by means of conductivity, viscometry, and light scattering studies.

Amphoteric surfactant has both a positive (cationic) and a negative (anionic) groups. It forms cations in acidic solution and shows anions in alkaline solution. In a middle of pH range, zwitterions are formed, i.e., molecules with two ionic groups of opposite charges. At this pH, the size of both positive charge and negative charge are equal and thus the net charge will be minimum (Lomax, 1996).

4.7.1 cmc and cac Measurements

Figure 4.59 shows the variation of the critical micelle concentration (cmc) with pH to determine the isoelectric point of CADG in aqueous solution. The surface tension of CADG as a function of CADG concentration graphs for each pH value are shown in Appendix (7.1). In this Figure, the cmc indicates a minimum at pH = 9 which is called the isoelectric point. As described earlier, there are equal numbers of positive charge and negative charge on the CADG micelles at the isoelectric point. Therefore, the cationic groups enhance to decrease the repulsion between negative charges, resulting in a closer packing of CADG micelles. Thus the surfactant molecules can aggregate easily at low CADG concentration. As a result, the cmc of CADG solution at isoelectric point shows minimum value as shown in Figure 4.59. Below and above the isoelectric point, the values of cmc are higher than that in the isoelectric point due to the increase of electrostatic repulsion between the charged headgroups. In this work, conductimetric, viscometric, and light scattering studies of the interaction between HPC and CADG were carried out at pH = 9 (isoelectric point) throughout the measurement.

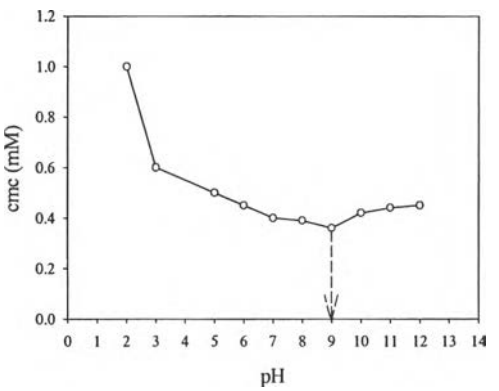

Figure 4.59 Dependence of critical micelle concentration (cmc) on pH at 30°C for amphoteric surfactant (CADG) solutions.

Figure 4.60 shows the conductivity of CADG at isoelectric point as a function of CADG concentration in the presence of HPC. The onset of a sudden change in the plot was determined to be a critical aggregation concentration (cac). As shown in Figure 4.60, the cac value (0.35 mM) is unchanged compared to the cmc value (0.36 mM). Brackman and Engberts (1994) also found that PEO has no effect on the cmc of zwitterionic surfactants, such as, protonated DDAO (dodecyldimethylamine-oxide). This criterion appears to resemble the complex formation between a neutral polymer with a nonionic surfactant. In such a complex system, the cmc value of nonionic surfactant is unchanged by the presence of polymer (Brackman *et al.*, 1988). These authors point out the fact that the cmc of the nonionic surfactant remains unchanged in the presence of polymer does not exclude the possibility of polymer-micelle complexation. The conductivity dramatically increases above cac due to the presence of large amount of ionic solution. In this range, the net charge on the micelle is larger than that on the free surfactant molecules.

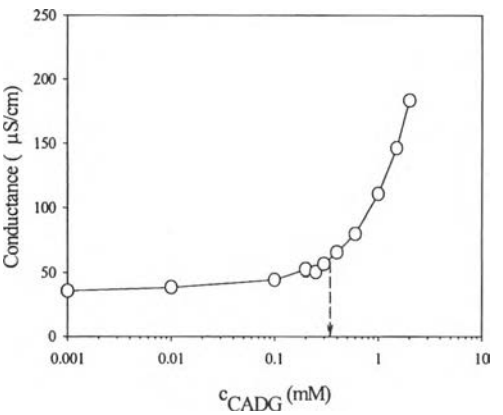

Figure 4.60 The variation of conductivity of CADG in the presence of HPC as a function of CADG concentration at pH = 9. HPC concentration = 0.4 g/dL.

4.7.2 Viscosity Measurement

Figure 4.61 indicates a plot of the specific viscosity (η_{sp}) as a function of CADG concentration at isoelectric point (pH = 9). The HPC concentration was fixed at 0.4 g/dL. This figure can be divided into 3 different regions.

Regions (I): The specific viscosity shows a gradual increasing trend with increasing CADG concentration up to a certain maximum value, which appears to correlate to the point at which the surfactant molecules start to form micelle (cmc = 0.36 mM).

Region (II): Beyond this maximum value, a decrease in η_{sp} was observed. We propose that, with further addition of surfactant, electrostatic attractions between positive and negative bound charges within the complex induce a strong reduction in hydrodynamic volume of the polymer and thus reduce the specific viscosity. As shown in Figure 4.61, a minimum in viscosity occurs at ~ 5 mM. Presumably, at this point, the HPC chain is saturated with CADG surfactant.

Region (III): At very high surfactant concentration, the specific viscosity increases very rapidly due to the structural changes of surfactant micelles (sphere to rod-like micelles) (Lomax, 1996).

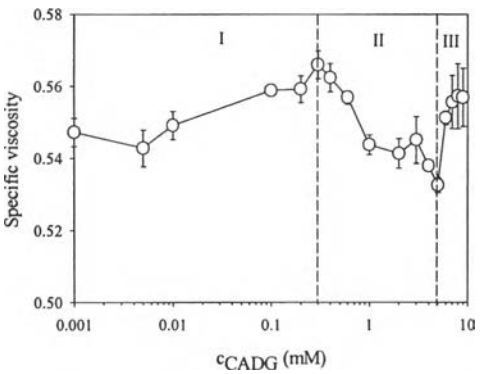

Figure 4.61 The specific viscosity (η_{sp}) as a function of CADG concentration at 30°C for HPC-CADG system at pH = 9. HPC concentration = 0.4 g/dL.

4.7.3 Hydrodynamic Radius Measurement

Figure 4.62 shows the apparent hydrodynamic radius (R_h) as a function of CADG concentration at isoelectric point. The hydrodynamic radius for each CADG concentration was calculated from the center of mass diffusion coefficient by using the Stokes-Einstein equation (equation 3.40).

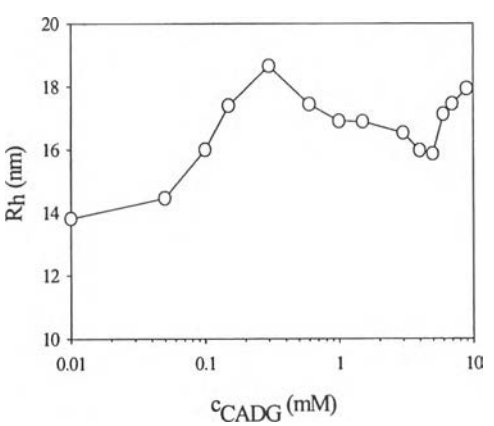

Figure 4.62 The apparent hydrodynamic radius (R_h) of HPC as a function of CADG concentration at pH = 9 for HPC-CADG system.

The corresponding graphs for the determination of R_h values are displayed in Appendix (7.4). The trend shown in this graph are generally consistent with those of the viscosity measurement. Again, a reduction of R_h was observed at $c_s/c_p = 0.43$ due to the binding between HPC and CADG. Above ~ 5mM CADG, the R_h increases because of the structural changes of CADG at high CADG concentration.

4.7.4 Determination of the Structure of HPC-CADG System

The structure of HPC-CADG system was determined by light scattering analysis using equation (3.27). The measurements were carried out at two different surfactant to polymer concentration ratios ($c_s/c_p = 0.026$; and $c_s/c_p = 0.43$), which refers to the minimum and maximum points as shown in viscostiy and R_h measurements. The Zimm plots for the HPC-CADG solution at $c_s/c_p = 0.026$, and $c_s/c_p = 0.43$ are displayed in Figures 4.63 and 4.64.

The corresponding dn/dc values at constant chemical potential were obtained via dialysis, which were determined to be 0.1214 mL/g and 0.1394 mL/g for the two concentration ratios ($c_s/c_p = 0.026$, and 0.43). From the Zimm plot analysis, the molecular weights of HPC in the ternary system of HPC-CADG system were obtained via equation (3.27). The molecular weights of HPC-CADG complex were calculated from equation (3.28). The results are tabulated in Table 4.10. The preferential interactions (D') of CADG with HPC at different mass concentration ratios were also determined via equation (3.11), calculated from the values of different (dn/dc) values by using equations (3.9) and (3.10). Then, $M_{w,com}$ was computed from equation (3.28). The values of the number of bound CADG molecules per HPC chain, as determined by $N_{s,b}/N_p = D' M_{w,HPC}/M_{CADG}$, where $M_{w,HPC} = 99{,}500$, and $M_{CADG} = 342$ g/mol, are also listed in Table 4.9 and compared with N_s/N_p, the total number of CADG molecules (bound + free CADG molecules) per HPC chain.

As indicated in Table 4.10, the preferential binding of CADG to HPC ($D' = 0.007$) shows nearly zero at $c_s/c_p = 0.026$. Again, $M_{w,com}$ at $c_s/c_p = 0.026$ (105,000 g/mol) is comparable with the molecular weight of HPC (99,500 g/mol). These data confirms that there is no interaction between HPC and CADG at this

ratio. However, the specific viscosity and R_h slightly increase at $c_s/c_p = 0.026$ up to the cmc ~ 0.36 mM. This cannot therefore be due to the formation of the surfactant micelles. The origin of the effect is unknown at present. At $c_s/c_p = 0.43$, the radius of gyration (R_g) decreases, which is generally consistent with the results of viscosity and dynamic light scattering measurements that a decrease in η_{sp} and R_h is observed beyond the maximum value ($c_s/c_p = 0.026$) as shown in Figures 4.61 and 4.62.

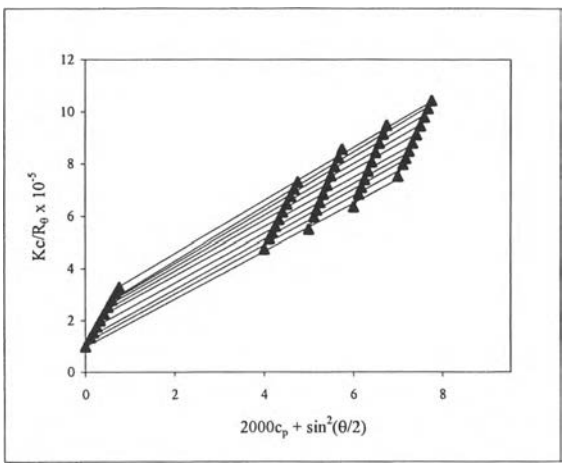

Figure 4.63 Zimm plot for HPC-CADG system at $c_s/c_p = 0.026$.

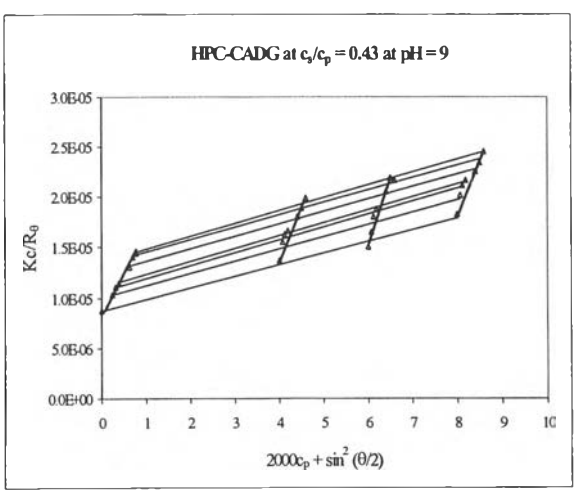

Figure 4.64 Zimm plot for HPC-CADG system at $c_s/c_p = 0.43$.

The molecular weight of HPC-CADG complex ($M_{w,com}$) at c_s/c_p = 0.43 (151,000 g/mol) increases, compared to the molecular weight of HPC (99,500 g/mol). Here, the preferential binding of CADG to HPC was determined as D' = 0.35, indicating that there is a significant binding between HPC and CADG at c_s/c_p = 0.43 g CDAG/g HPC. In contrast with the ionic surfactants, the amphoteric surfactant has both positive charge and the negative charge in the same surfactant molecule, and therefore, electrostatic attractions between positive and negative charges on bound micelles occur within the polymer chain. This would induce a strong reduction in hydrodynamic volume of the HPC chain and thus reduce the R_g and R_h of the HPC-CADG complex system at c_s/c_p = 0.43.

Table 4.10 Physical parameters of HPC-CADG complexes at different c_s/c_p ratios, determined by refractive index and light scattering measurements

Physical parameters	HPC-CADG at c_s/c_p = 0.026	HPC-CADG at c_s/c_p = 0.43
$(dn/dc_p)_{\mu s}$ (mL/g)	0.1214 ± 0.002	0.1394 ± 0.002
$(dn/dc_p)_{cs}$ (mL/g)	0.1205 ± 0.001	0.1029 ± 0.003
$(dn/dc_s)_{cp}$ (mL/g)	0.1240 ± 0.003	0.1027 ± 0.003
D'	0.007	0.355
$M_w \times 10^{-5}$ (g/mol)	1.04 ± 0.09	1.12 ± 0.01
$M_{w,com} \times 10^{-5}$ (g/mol)	1.05 ± 0.13	1.52 ± 0.02
R_h (nm)	18.65 ± 2.6	15.85 ± 2.8
R_g (nm)	55.6 ± 3.6	52.1 ± 0.35
N_s/N_p	8	125
$N_{s,b}/N_p$	2	102
# of HPC chain	1.0 ± 0.002	1.3 ± 0.002